AGU PUBLICATIONS

JGR

Journal of Geophysical Research: Planets

RESEARCH ARTICLE

10.1002/2014JE004642

Key Points:
- Reappraisal of the Martian crust density
- Martian basalt density ranges from 3100 to 3300 kg/m^3
- Existence of buried felsic component in the Noachian highlands

Correspondence to:
D. Baratoux,
david.baratoux@get.obs-mip.fr

Citation:
Baratoux, D., H. Samuel, C. Michaut, M. J. Toplis, M. Monnereau, M. Wieczorek, R. Garcia, and K. Kurita (2014), Petrological constraints on the density of the Martian crust, *J. Geophys. Res. Planets*, *119*, 1707-1727, doi:10.1002/2014JE004642.

Received 5 APR 2014
Accepted 11 JUN 2014
Accepted article online 13 JUN 2014
Published online 31 JUL 2014

Petrological constraints on the density of the Martian crust

David Baratoux[1,2], Henri Samuel[3,4], Chloé Michaut[5], Michael J. Toplis[3,4], Marc Monnereau[3,4], Mark Wieczorek[5], Raphaël Garcia[3,6], and Kei Kurita[7]

[1]Université de Toulouse, UPS-OMP, GET, Toulouse, France, [2]IRD/Institut Fondamental d'Afrique Noire, Dakar, Senegal, [3]Université de Toulouse, UPS-OMP, IRAP, Toulouse, France, [4]CNRS; IRAP; 14, avenue Edouard Belin, F-31400 Toulouse, France, [5]Institut de Physique du Globe de Paris, Université Paris Diderot, Sorbonne Paris Cité, France, [6]Ecole nationale suprieure de l'aronautique et de l'espace, Toulouse, France, [7]Earthquake Research Institute, University of Tokyo, Tokyo, Japan

Abstract New insights into the chemistry of the Martian crust have been made available since the derivation of crustal thickness maps from Mars Global Surveyor gravity and topography data that used a conservative range of density values (2700–3100 kg/m^3). A new range of crustal density values is calculated from the major element chemistry of Martian meteorites (3100–3700 kg/m^3), igneous rocks at Gusev crater (3100–3600 kg/m^3) and from the surface concentration of Fe, Al, Ca, Si, and K measured by the Gamma-Ray Spectrometer on board Mars Odyssey (3250–3450 kg/m^3). In addition, the density of mineral assemblages resulting from low-pressure crystallization of primary melts of the primitive mantle are estimated for plausible conditions of partial melting corresponding to the Noachian to Amazonian periods (3100–3300 kg/m^3). Despite the differences between these approaches, the results are all consistent with an average density above 3100 kg/m^3 for those materials that are close to the surface. The density may be compatible with the measured mass of Mars and the moment of inertia factor, but only if the average crustal thickness is thicker than previously thought (approaching 100 km). A thicker crust implies that crustal delamination and recycling could be possible and may even control its thickness, globally or locally. Alternatively, and considering that geoid-to-topography ratios argue against such a thick crust for the highlands, our results suggest the existence of a buried felsic or anorthositic component in the southern hemisphere of Mars.

1. Introduction

Terrestrial planets and some of the largest asteroids are known to be chemically differentiated into a dense metallic core, a silicate mantle, and a crust [e.g., *Ringwood*, 1966; *Solomon*, 1980; *Russell et al.*, 2012]. Such large-scale chemical differentiation requires one or several sources of energy, such as high-velocity impacts, or the heat provided by the decay of radiogenic elements, with the physical separation of metal and silicate phases being driven by density contrasts and gravity forces. With the exception of material at the surface of partially differentiated asteroids that may escape melting [*Weiss and Elkins-Tanton*, 2013], the term crust generally applies to the outermost envelope extracted from the silicate mantle through melting and separation of solid-liquid phases. This definition encompasses a large spectrum of possible scenarios. For example, a primary crust may start to form as the result of the crystallization of a magma ocean. Even here, one should distinguish between crustal rocks formed by segregation of minerals from the magma ocean due to their density contrast with the liquid (e.g., plagioclase floatation crust and mantle cumulates in the case of the Moon) and partial melting of upper regions of the mantle as a consequence of mantle overturn, as proposed for the case of Mars [*Elkins-Tanton et al.*, 2005; *Elkins-Tanton*, 2012]. A basaltic crust from Mg-rich and Al-poor mantle cumulate sources would form in the second case. Prolonged crustal growth (secondary crust) is possible if internal energy is sufficient to maintain the existence of zones of partial melting at depths where magma is buoyant and to bring fertile mantle into these regions. These partial melts may ascend to the surface and produce volcanic eruptions or may intrude into the crust, adding in both cases to its volume. Internal differentiation of the secondary crust through recycling and remelting of its components is referred to as a tertiary crust [*Taylor*, 2012]. Early (primary) crustal material, through various mechanisms of recycling into the mantle, may be partially or totally removed, as observed on Earth. Therefore, the age of crustal materials span the entire range from solar system formation to the present day, but the rocks exposed at the surface of terrestrial planets offer more or less limited time windows into the history of crustal growth.

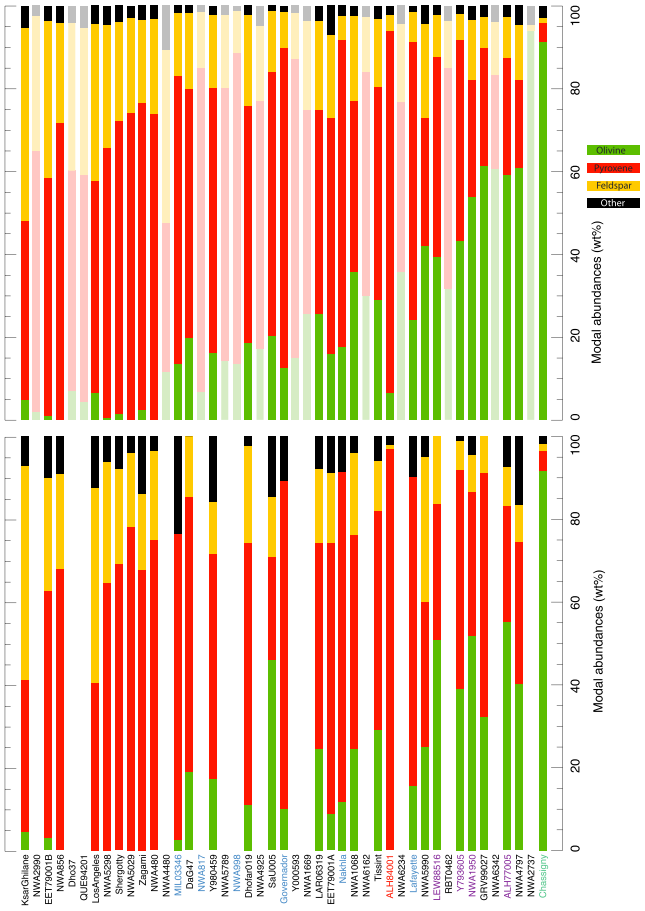

Figure 1. (top) Feldspar, pyroxene, and olivine concentration obtained from CIPW norm for averaged bulk rock chemical composition of Martian meteorites. (bottom) Observed concentrations of feldspar, pyroxene, and olivine as given by the Martian Meteorite Compendium [*Meyer*, 2012]. The comparison confirms that the normative mineralogy is in reasonable agreement with observed mineralogy for the major phases. Samples for which the observed normative mineralogy is not available are shown with reduced intensity to facilitate comparison for the others. Samples are arranged by increasing density as given using the CIPW norm.

In this respect, Mars has a long and rich volcanic history [*Grott et al.*, 2013] but has also preserved old crustal material, exposed essentially in the southern hemisphere. The nature of these ancient igneous rocks is debated. Initially seen as the components of a primary crust (magma-ocean related) [*Elkins-Tanton et al.*, 2005], their composition appears now to be compatible with a period of intense volcanism (secondary crust) associated with high (> 18 wt %) degrees of partial melting of the mantle [*Baratoux et al.*, 2013]. Despite insights into surface composition and crustal structure provided by the Martian meteorites and by remote sensing and in situ observations, it is indeed not known if Mars has preserved a significant proportion of its primary (magma-ocean related) crust or if the crustal growth through the subsequent addition of partial melts of the mantle accounts for most of the crustal volume. In other words, it is not known if Mars is similar to the Moon or to the Earth in this respect.

In addition to chemical and mineralogical data, inversion of geophysical data (moment of inertia, average density, or gravity field) provides constraints on the distribution of mass in a planet and therefore on crustal thickness and density. However, the number of unknowns in this approach is large. Geophysical parameters were estimated and analyzed before strong petrological constraints were available. As a consequence, conservative assumptions concerning crustal density were generally made. Despite the fact that Martian meteorites were known to be generally denser than 3200 kg/m^3 a range of average crustal density limited to 2700–3100 kg/m^3 was preferred [*Zuber*, 2001; *McGovern et al.*, 2002; *Neumann et al.*, 2004; *Wieczorek and Zuber*, 2004; *Sohl et al.*, 2005]. These values were also influenced by a high-silica composition given by Pathfinder analyses [*Nimmo and Tanaka*, 2005]. The Martian meteorites were considered to be a nonrepresentative set of samples of the Martian crust biased toward young ages.

Ten years later, these hypotheses need to be revisited in light of the newly available constraints. For example, the young age of the basaltic shergottites has been contested [*Bouvier et al.*, 2009, 2014] even if recent studies tend to favor young crystallization ages [*Moser et al.*, 2013; *Zhou et al.*, 2013]. The number of chemical analyses on Martian meteorites has increased significantly since the last survey made by *Lodders* [1998], and new samples of Mars have reached our planet [*Chennaoui-Aoudjehane et al.*, 2012]. In addition, numerous chemical and mineralogical observations on the Martian crust have been made at a variety of spatial scales [*Grott et al.*, 2013]. We therefore propose a reappraisal of the crustal density of Mars and argue that the basaltic component of the Martian crust has a density above 3100 kg/m^3. If this density is representative of the entire crust, it would imply a threefold reduction of the density contrast with the mantle in comparison to previous studies. We then compare these results with geophysical constraints

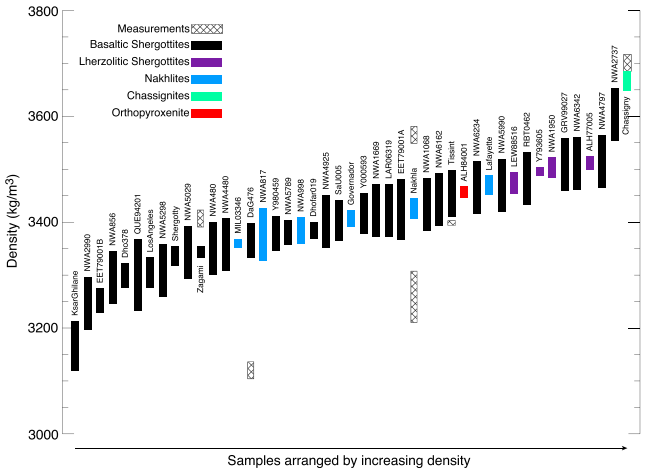

Figure 2. Density of the Martian meteorites estimated from bulk chemistry and CIPW norm. Samples are arranged by increasing density. Laboratory measurements [*Consolmagno and Britt*, 1998; *Coulson et al.*, 2007; *Britt et al.*, 2012] of grain densities are represented for comparison.

and discuss the implications for the structure of the crust, its recycling, and for the presence of a buried component.

2. Density of the Martian Meteorites

Straightforward constraints on crustal density come from direct measurements of the density of Martian meteorites. However, such analyses are surprisingly rare and provide values for only a few samples [*Consolmagno and Britt*, 1998; *Coulson et al.*, 2007; *Britt et al.*, 2012]. Given the small masses analyzed, the actual error bars for a given sample are likely to be underestimated in these studies. Another approach consists in calculating the density of the normative mineralogy inferred from bulk geochemistry [*Lodders*, 1998; *Neumann et al.*, 2004]. As previously noted by *Lodders* [1998], it is shown here that normative mineralogy compares well with observed mineralogy in the case of Martian meteorites. Therefore, this approach provides a good estimate of the grain density. New analyses have been made on the Martian meteorites since the normative calculations of *Lodders* [1998], and a new compilation of the bulk rock chemistry for the major elements (SiO_2, MgO, FeO, Al_2O_3, CaO, MnO, K_2O, Na_2O, TiO_2, and Cr_2O_3) was made for this purpose.

We then calculated the CIPW norm from individual analysis (up to 10 analyses per samples) and known mineral densities from *Robie and Hemingway* [1995]. The CIPW norms were calculated following the set of rules given by *Hutchison* [1975]. The CIPW norm is a tool providing a theoretical mineral assemblage for igneous rocks that is based on a set of simple mass balance constraints and a limited set of minerals. It may result in simplified mineral assemblages and compositions and does not provide any information on the possibility for zoned minerals, for example. Despite these limitations, we confirm that the normative mineralogy is reasonably similar to the actual mineralogy of each sample (when observations are available) (Figure 1). An average density and standard deviation was then calculated for each sample. When only one chemical analysis was available, an arbitrary error bar of 100 kg/m^3 was assigned (greater than the error bars on samples where more analyses by multiple authors are available). The densities are then represented in increasing order (Figure 2), and the laboratory measurements are shown for comparison. The densities of Martian meteorites calculated in this way (at 1 bar and 25°C) range from less than 3200 kg/m^3 to more than 3600 kg/m^3 with values around 3300–3500 kg/m^3 for most of the basaltic shergottites.

An alternative way to obtain a theoretical mineral assemblage from bulk rock chemistry is to simulate equilibrium crystallization down to the solidus using a thermodynamic calculator such as MELTS [*Ghiorso and Sack*, 1995]. Even this approach simplifies the potentially complex history of a given sample that may include degrees of fractional and polybaric crystallization and/or crystal accumulation, kinetic effects, and subsequent alteration. Equilibrium crystallization calculations were performed using the latest optimized version of the original MELTS software [*Gualda et al.*, 2014]. This version (rhyolite-MELTS) has been developed to include silica-rich and fluid-bearing systems [*Gualda et al.*, 2014], but it uses the same calibration for basaltic compositions as the original MELTS calculator [*Ghiorso and Sack*, 1995], having the advantage of being numerically more stable [*Gualda et al.*, 2014].

As for the CIPW norm, a comparison of the (average) calculated mineralogy with actual mineralogy is given (Figure 3). Several densities were calculated using the various analyses for a given sample, and the average value and its standard deviation were then calculated. The effect of oxygen fugacity on density was checked by varying the crystallization conditions between 3 log units and 1 log unit below the Quartz-Fayalite-Magnetite buffer that represents the inferred range of oxygen fugacity conditions for the

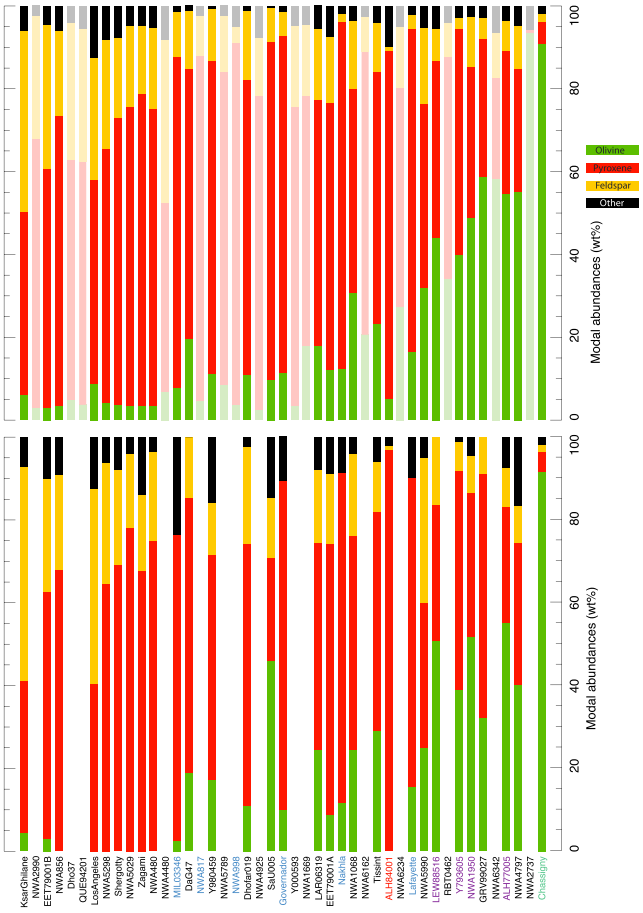

Figure 3. (top) Feldspar, pyroxene, and olivine concentration obtained calculated with MELTS assuming equilibrium crystallization with oxygen fugacity 2 log units below the QFM buffer. (bottom) Observed concentrations of feldspar, pyroxene, and olivine as given by the Martian Meteorite Compendium [*Meyer*, 2012]. Samples are arranged as in Figure 1, by increasing density, as given by the CIPW norm. Samples for which the observed normative mineralogy is not available are shown with reduced intensity to facilitate comparison for the others.

Martian meteorites [*Grott et al.*, 2013]. The density values were then represented in increasing order with the laboratory measurements (Figure 4). A similar range of density is found using this method to that derived from normative calculations. In detail, an average difference of 80 kg/m^3 is found between thermodynamic and normative calculations (with a standard deviation of 60 kg/m^3). The effect of variable oxygen fugacity is less than a few tens of kg/m^3.

3. Density of Surface Rocks: Constraints From In Situ and Remote Sensing Observations

3.1. In Situ Observations

Another constraint on the density of crustal rocks may be derived from in situ observations of surface rocks. The main source of information is given by the Athena science payload of the two Mars Exploration Rovers, Opportunity and Spirit [*Squyres et al.*, 2003]. The rover Opportunity has driven more than 5 km across Meridiani Planum. It has mainly investigated sedimentary rocks, such as sandstones composed of sulfates, hematitic-rich concretions, and a matrix of fine-grained siliclastics produced by the alteration of an olivine basalt [*Squyres et al.*, 2006]. The bulk crust of Mars being largely dominated by igneous material; these observations are not directly relevant to our objective, with the exception of Bounce rock, a loose rock having affinities with lithology B of the shergottite meteorite EETA79001 [*Squyres et al.*, 2006; *Zipfel et al.*, 2011]. The second rover, Spirit, landed on a volcanic unit in the floor of Gusev crater dominated by olivine-bearing basalts [*Arvidson et al.*, 2006]. The felsic rocks measured by Pathfinder [*Brückner et al.*, 2003] and the first chemical analyses at Gale crater [*Stolper et al.*, 2013; *Schmidt et al.*, 2014] are also included for comparison with MER data.

As with Martian meteorites, these data provide a very restricted sampling of the potential diversity of crustal igneous rocks. However, while Martian meteorites have Amazonian or Noachian crystallization ages, some rocks analyzed on the floor of Gusev crater (Adirondack-class basalts) were formed during the Hesperian period [*Greeley et al.*, 2005], therefore providing potential insights into density variations with time.

No direct in situ density measurements were performed by the Athena science payload. However, the bulk composition of rocks are provided by an Alpha Particle X-ray Spectrometer (APXS) [*Ming et al.*, 2008]. In addition, iron-bearing minerals were detected by a Mössbauer spectrometer [*Morris et al.*, 2006, 2008] and iron-bearing or iron-free major phases were characterized by a Miniature Thermal Infrared Spectrometer (Mini-TES) [*Ruff et al.*, 2006]. Bulk rock chemical compositions may be recast into normative mineralogy, from which an estimate of the pore-free density may be calculated. *McSween et al.* [2008] have shown that normative olivine, pyroxene, and feldspar proportions and compositions calculated from APXS data are

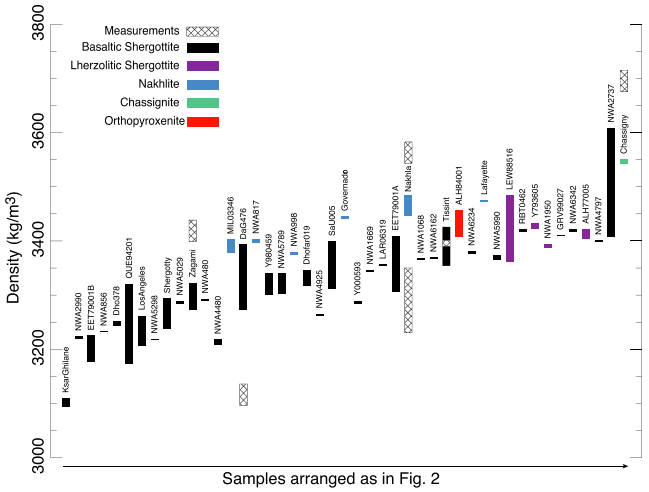

Figure 4. Density of the Martian meteorites estimated from bulk chemistry and calculated equilibrium crystallization with MELTS [*Ghiorso and Sack*, 1995]. Sorted are arranged as in Figure 2 (increasing density, as given using the CIPW norm). Laboratory measurements from *Consolmagno and Britt* [1998], *Coulson et al.* [2007], and *Britt et al.* [2012] of grain densities are represented for comparison.

consistent with the MINI-TES spectroscopic constraints. As the relative abundances of these three major phases control the density value, a similar approach has been applied here to the rocks cleaned with the Rock Abrasion Tool (RAT) or "RAT-ed" rocks. The density from each APXS analysis is calculated, as for the Martian meteorites, using mineral density values at standard conditions [*Robie and Hemingway*, 1995]. Errors on density values are calculated from the propagation of estimated APXS errors for major oxides (SiO_2, TiO_2, Al_2O_3, CaO, MgO, FeO, K_2O, TiO_2, and Cr_2O_3). In detail, a population of bulk compositions has been generated for each sample, assuming the random errors on the major oxides are independent and follow a Gaussian distribution.

However, our objective was not to reproduce the mineralogy of individual samples, but rather to explore the range of possible densities of crustal rocks from the diversity of compositions observed at Gusev (and Bounce rock from Meridiani). Surface rocks are often altered, more or less oxidized, and include a variable amount of volatile species, determined by the initial conditions of formation and the subsequent history of fluid-rock interactions. The concentration of volatile species and the Fe^{3+}/Fe_T ratio measured at the surface are not necessarily representative of unaltered subsurface rocks and may induce a bias in the calculated densities with respect to their unaltered counterparts. Sulfur and chlorine in Gusev rocks may be the result of condensation of volcanic exhalations or alternatively included in secondary minerals that precipitated from fluids [*McSween et al.*, 2008]. In the first case, sulfur and chlorine should be subtracted as SO_3 and Cl, whereas accompanying cations should be removed in the second case (e.g., $MgSO_4$, NaCl). The comparison of norms obtained assuming precipitation of secondary minerals with spectroscopic constraints reveals several problems [*McSween et al.*, 2008]. Sulfur and chlorine were therefore removed as SO_3 and Cl before calculating their normative mineralogy. The removal of these two elements does not affect the density calculations by more than 10 kg/m^3. On the other hand, the

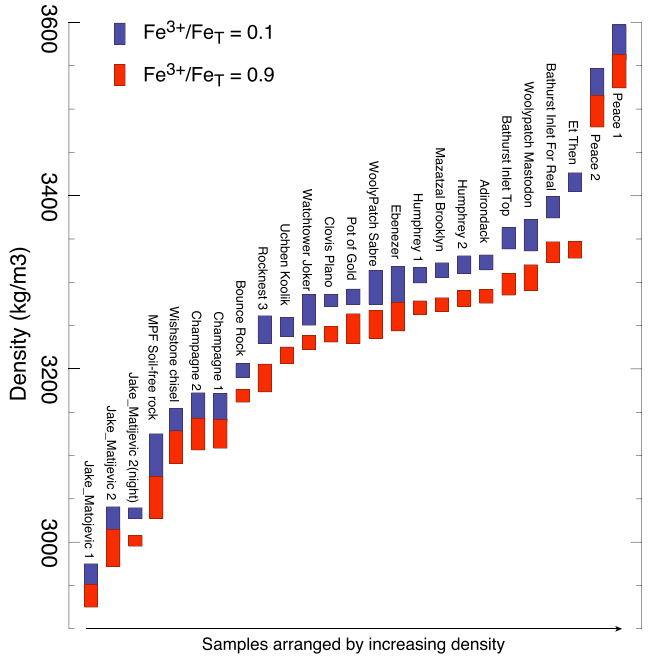

Figure 5. Density of igneous rocks at Mars Pathfinder landing site (MPF soil-free rocks), Gale crater (Jake Matijevic, Bathurst Inlet, Et Then, Rocknest 3), Meridiani (Bounce rock), and Gusev crater (all others data) estimated from CIPW norm and APXS S-free and Cl-free measurements. Rocks were cleaned using the Rock Abrasion Tool of the Mars Exploration Rovers for Gusev Crater and Meridiani. Density is calculated for two extreme conditions of oxidations.

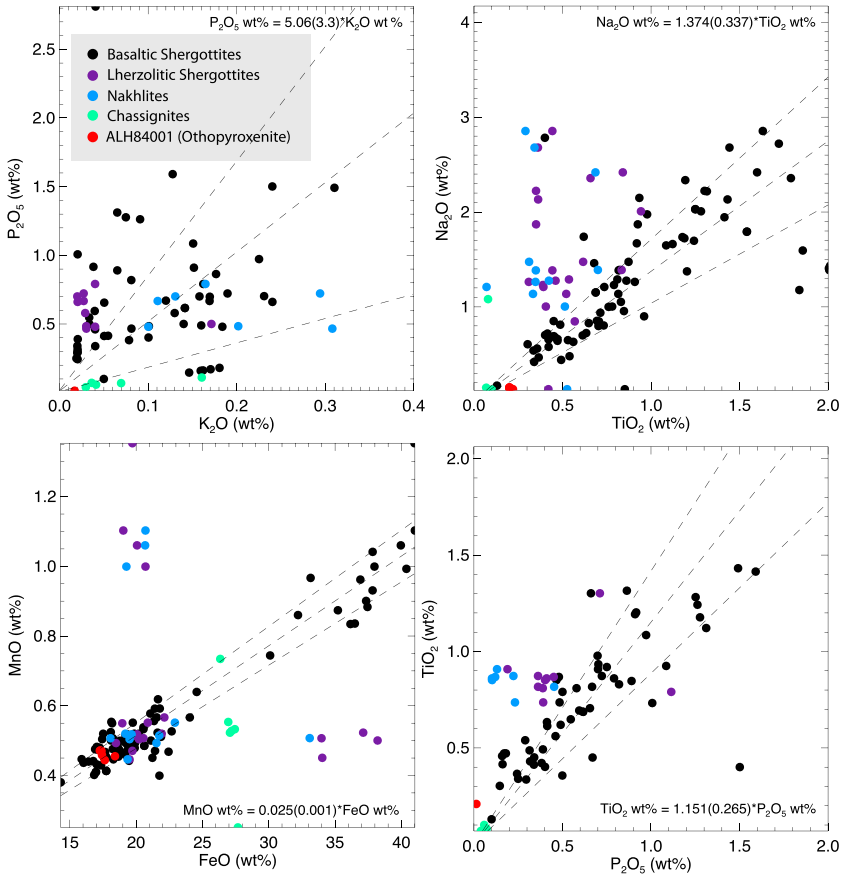

Figure 6. Ratio of selected chemical elements (in oxide wt %) in Martian meteorites. Chemical trends are given for the basaltic shergotties. Bulk compositions are from the Mars Meteorite Compendium [*Meyer*, 2012]. Least squares adjustment for each trend is reported (with error bars) and displayed as dotted lines (measurements with $K_2O < 0.6$ wt % are excluded for the calculation of the P_2O_5/K_2O ratio.

Fe^{3+}/Fe_T molar ratio measured by the Mössbauer spectrometer varies from < 0.2 for nearly unaltered rocks (e.g., Adirondack) to 0.6–0.9 for pervasively altered samples [*Morris et al.*, 2006]. The Martian crust should be dominated by unaltered rocks, with $Fe^{3+}/Fe_T < 0.2$. In order to illustrate the maximal influence of this parameter, the density calculations were performed for two values of the Fe^{3+}/Fe_T ratio, of 0.1 and 0.9. The results are shown in Figure 5. Density values for basaltic samples (including Bathurst at Gale crater) range from 3100 kg/m^3 to about 3600 kg/m^3 with a cluster at 3200–3300 kg/m^3. Such a range of values is very similar to that inferred from the Martian meteorites. The only exceptions are Pathfinder felsic rocks and the Al-rich mugearite Jake_M at Gale that are significantly less dense than the basalts. Differences due to variations in oxidation state are smaller than 50 kg/m^3, even for the large range of conditions considered here.

3.2. Density From Geochemical Maps

Another source of information on crustal composition, and therefore density, is given from the Gamma-Ray Spectrometer (GRS) data on board Mars Odyssey [*Boynton et al.*, 2007]. Five degree resolution maps were released of the concentration of five rock-forming elements, Fe, Al, Ca, Si, K, and Cl, within the first tens of centimeters below the surface. The calculation of rock density from these data requires several assumptions that are presented below and discussed in the following paragraph.

The oxygen concentration is not measured, and the concentration of each chemical element is therefore converted into its oxide wt % assuming that all iron is in the Fe^{+2} oxidation state. It is likely that superficial material includes a soil/dust fraction with a proportion of volatile elements (Cl, S, and H_2O) that are not equally abundant in the deeper crust, and the wt % oxides were therefore normalized to a Cl-free and H_2O free composition. As seen before for the Martian meteorites, sulfur has little influence on the bulk density and is neglected. In any case, preliminary sulfur concentrations at the surface provided by GRS observations

Table 1. Ratios of Incompatible Elements in Basaltic Shergottites[a]

Ratio	Na_2O/TiO_2	TiO_2/P_2O_5	MnO/FeO	P_2O_5/K_2O
SNC	1.374	1.151	0.025	4.297
Error (1σ)	0.337	0.265	0.001	0.939
Other studies	1.55[b]	1.17[c]	0.0256[d]	–

[a]Ratios obtained by previous studies (from a smaller set of samples) are indicated for comparison.
[b]*Treiman et al.* [1986].
[c]*Treiman* [2003].
[d]*Dreibus and Wänke* [1985].

[*King and McLennan*, 2010] are associated with large error bars. Small quantities of sulfur in the form of sulfates or sulfides are present in the Martian crust. However, sulfates deposits are superficial and would not affect the average density of the Martian crust (see discussion below on the roles of secondary phases) and the small amount of (dense) sulfides in igneous rocks has little influence on bulk rock density. Chromium is generally below 1 wt % and was also neglected.

The abundance of one major element, magnesium, is unknown. In addition, the abundance of Na, Ti, P, Cr, and Mn that generally accounts for about or less than 10 wt % of a basaltic rock is not available. TiO_2, P_2O_5, MnO, and Na_2O have, to first order, an incompatible behavior during partial melting and/or crystallization, and it is of note that P_2O_5/K_2O, Na_2O/TiO_2, MnO/FeO, and TiO_2/P_2O_5 ratios are approximately constant when considering the group of basaltic shergottites (Figure 6). The average values of these ratios and their standard deviations in basaltic shergottites are given in the Table 1. The table includes ratios from previous studies using a smaller set of samples for comparison. The surface abundances of TiO_2, P_2O_5, MnO, and Na_2O may be therefore estimated using the average values of these ratios in the basaltic shergottites and the measured K_2O surface concentration from GRS. Assuming that the sum of all major elements is 100% of which only MgO is unknown, a map of magnesium concentration can then be derived (Figure 7). A normative (CIPW) mineralogy, following the same rules as for the other chemical data sets, is then calculated. This exercise produces mineral assemblages dominated by plagioclase, olivine, and the frequent occurrences of two pyroxenes, in overall agreement with visible and near infrared observations. For each pixel of the map, the density of each assemblage is calculated from mineral densities at 25°C and 1 bar [*Robie and Hemingway*, 1995].

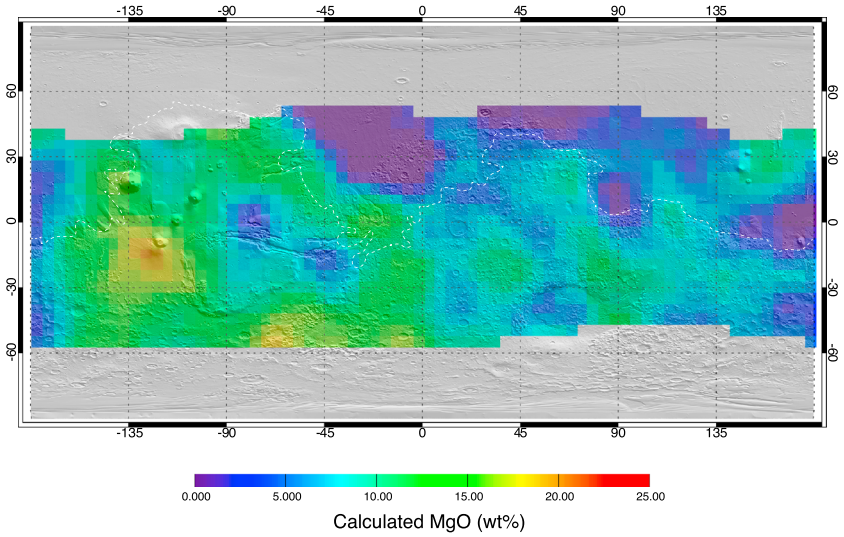

Figure 7. Concentration of MgO at the surface of Mars calculated by difference from GRS geochemical maps for FeO, Al_2O_3, CaO, SiO_2, K_2O and elemental ratios in Martian meteorites for other major oxides (P_2O_5, TiO_2, Na_2O, MnO). The dotted white line represents the dichotomy boundary defined from crustal thickness [*Watters et al.*, 2007].

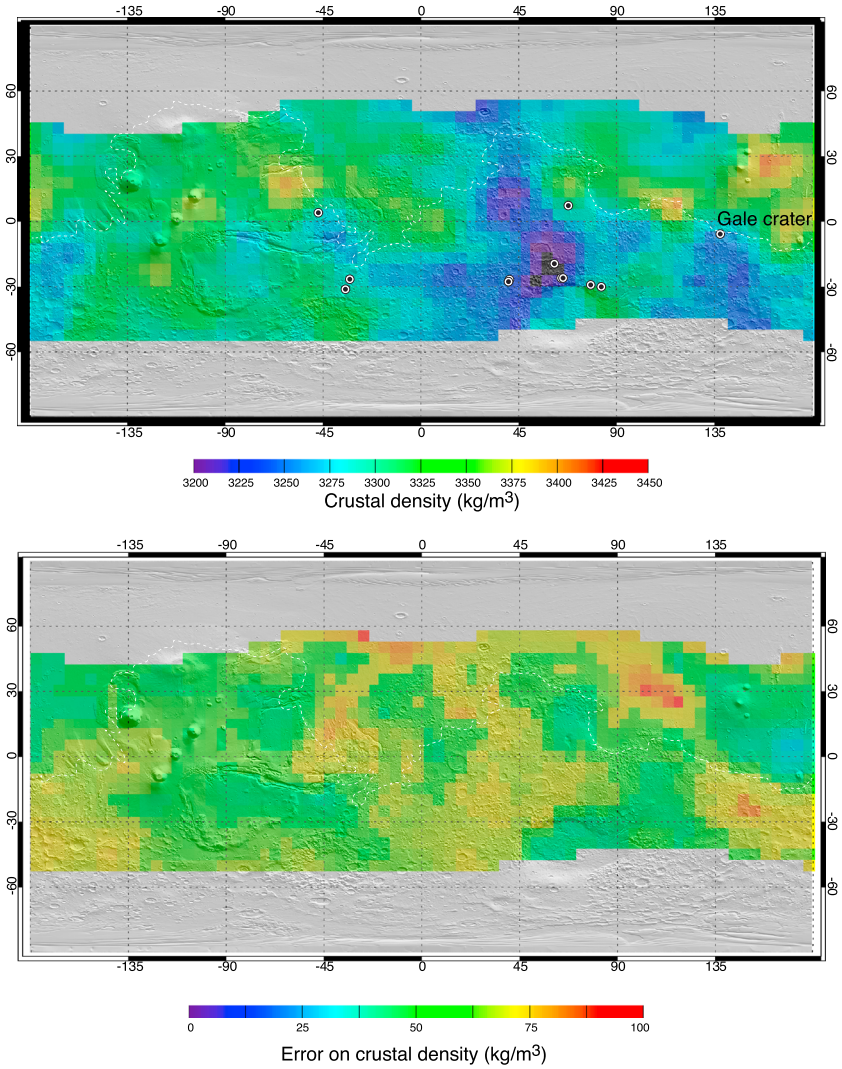

Figure 8. (top) Density map of surface rocks estimated from CIPW norm using GRS geochemical maps of FeO, Al_2O_3, CaO, SiO_2, K_2O, and constant ratios in Martian meteorites for other major oxides (P_2O_5, TiO_2, Na_2O, MnO). Black/white circles correspond to locations where felsic/anorthositic rocks have been possibly identified using spectroscopic data [*Carter and Poulet*, 2013; *Wray et al.*, 2013] or have been documented by in situ analyses (Gale crater) [*Sautter et al.*, 2014]. (bottom) Formal error on the density map associated with the error bars on the elemental ratios. The dotted white line represents the dichotomy boundary defined from crustal thickness [*Watters et al.*, 2007].

The density map of surface rocks estimated following this approach is shown in Figure 8, and the corresponding histogram of densities is given in Figure 9. Variations in the density map principally reflect the estimated proportion of mafic minerals relative to feldspar. Higher-density regions are mostly in Hesperian and Amazonian volcanic units. Lower density regions are found in the Noachian crust around the Hellas and Argyre basins, and in the chaotic terrains. It is of note that these locations correspond to places where Noachian Fe-plagioclase/anorthosites have been identified using Compact Reconnaissance Imaging Spectrometer for Mars (CRISM) orbital data [*Carter and Poulet*, 2013; *Wray et al.*, 2013] (with the exception of the site in Syrtis Major that is likely related to minor volumes of evolved magmas following igneous differentiation). Gale crater, where feldspar-rich material and evolved magmas have also been identified in situ by the Curiosity rover [*Sautter et al.*, 2014], also belongs to the low- density regions of the map.

The validity of this approach has been tested using the Martian meteorites. Assuming that Fe, Al, Ca, Si, and K are the only known elemental concentrations for the meteorites, the other elements were calculated using average ratios, as for the GRS data, and the MgO was calculated by difference. The modal abundances for pyroxene, olivine, and feldspar calculated in this way agree well with modal abundances calculated using

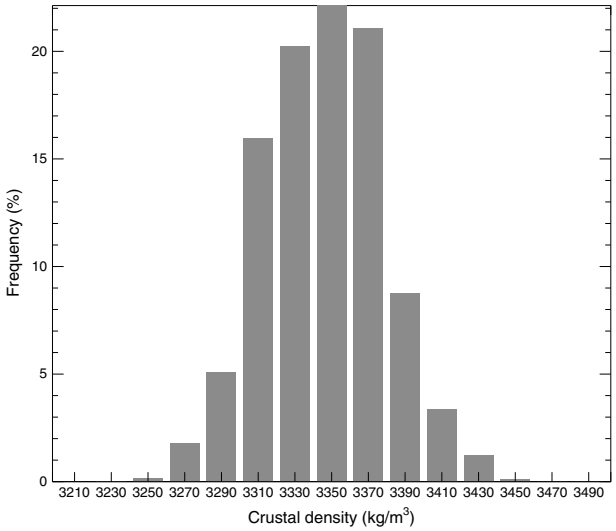

Figure 9. Histogram of density values obtained from CIPW norm on GRS chemical maps and constant element ratios for the other major oxides (P_2O_5, TiO_2, Na_2O, MnO). Density values calculated in this way range between 3200 kg/m^3 and 3450 kg/m^3 with a single peak at 3350 kg/m^3.

the known composition of each sample (Figures 10a–10c). Since the relative modal abundances of these phases is the primary factor controlling the density, the density of Martian meteorites calculated with a limited set of elements (and constant ratios for the other major elements) agrees well with their density calculated from the entire set of major elements (Figure 10f). The Mg# calculated by this approach show larger, but acceptable differences with the actual Mg# (up to 10) of each sample (Figure 10e). Modal abundances of oxide minerals are, however, not reproduced correctly (Figure 10d). This is likely due to the absence of Cr, errors on Ti, and to the redistribution of iron between silicates and iron

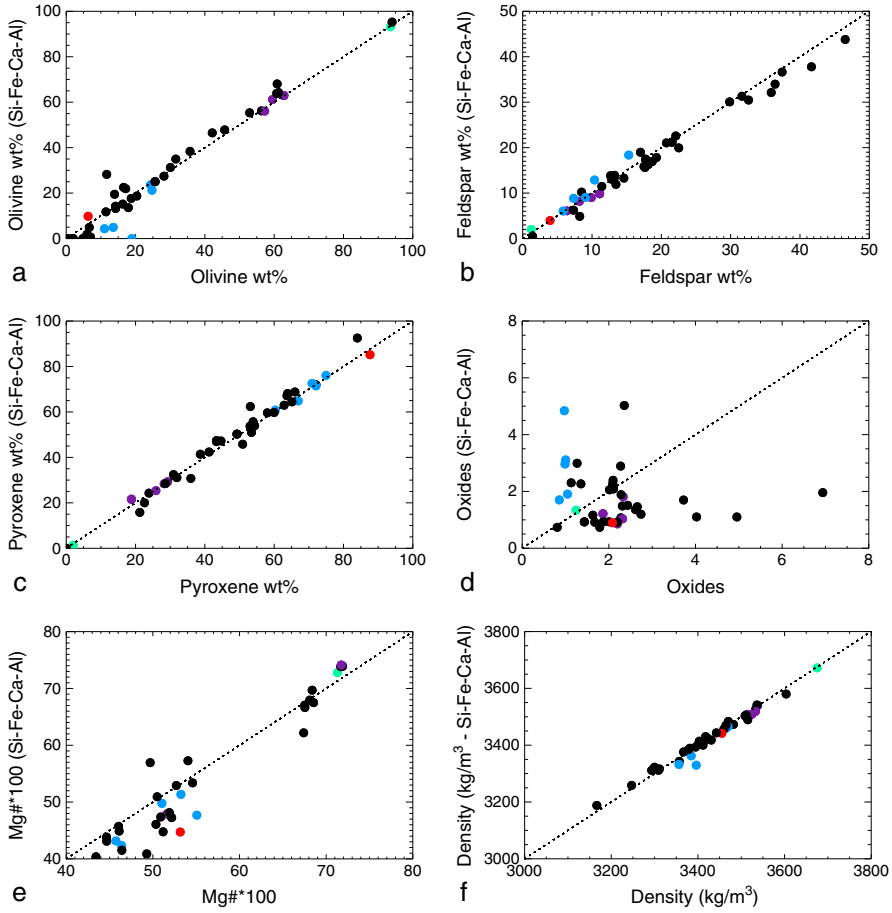

Figure 10. Modal abundances for (a) olivine, (b) feldspar, (c) pyroxene, (d) oxides (d), (e) Mg#*100 , and (f) grain density, calculated from FeO, Al_2O_3, CaO, SiO_2, and K_2O concentrations completed using, as for GRS data, constant ratios for the other oxides concentrations (P_2O_5, TiO_2, Na_2O, MnO) (*y* axis) versus calculations from the actual chemical composition of each sample (*x* axis).

Table 2. Composition of a Global Soil/Dust Material (wt %)

Oxides	SiO_2	CaO	Al_2O_3	FeO	K_2O	SO_3
Abundance	45.0	7.0	10.0	18.0	0.4	5.0

oxides as a result of the error on the inferred Mg#. However, given the small contribution of oxide minerals to the bulk density, this source of error does not affect our conclusions regarding density results.

There are several (potentially large) sources of uncertainties in the above calculation, including the GRS elemental abundances, the amount of oxygen (oxidation state), the average abundance of volatile elements in the crust relative to superficial material (including the unknown abundance of sulfur), and the error bars on P_2O_5/K_2O, Na_2O/TiO_2, MnO/FeO, and TiO_2/P_2O_5 ratios that propagate into the concentration of MgO. Some of these sources of errors may be examined and quantified in more detail. The P_2O_5/K_2O, Na_2O/TiO_2, MnO/FeO, and TiO_2/P_2O_5 ratios are varied according to their standard deviations assuming a Gaussian distribution, and a density map is calculated for each set of ratios. A formal error bar is then given for each pixel of the map from the standard deviation of density values (Figure 8), from which errors up to 60–80 kg/m^3 were obtained. Errors due to GRS measurements have been estimated in the same way, which adds another 25–80 kg/m^3 uncertainty.

The inferred Mg concentration of the crust (Figure 7) may be also examined. A large fraction of the Martian surface would have a Mg# between 40 and 70, as expected for an igneous crust extracted from a mantle with a Mg# of ~ 75, consistent with the value estimated by *Dreibus and Wänke* [1985]. This should be considered as a surprisingly good result given the limitations of our approach. However, a few Planitiae of the northern hemisphere, including Isidis, Elysium, Chryse, and Acidalia Planitia would have a Mg# less than 40 suggesting that elemental ratios for incompatible elements have been perturbed by postmagmatic processes such as aqueous alteration [*Taylor et al.*, 2006]. The widespread occurrence of more evolved magmas for which elemental ratios inferred from basaltic material would not apply is an alternative possibility, but is not really supported by independent (e.g., spectral) observations. The high wt % of MgO in a restricted region in the south of Tharsis is at odds with the small degree of partial melting inferred from iron and silica and expected for Amazonian volcanism [*El Maarry et al.*, 2009], suggesting the presence of another element. In any case, our approach is not considered valid for regions with anomalously low or high Mg# and the corresponding density calculations (which actually remain in the range of values calculated elsewhere) should not be considered valid.

The effect of neglecting the presence of a homogeneous soil component in superficial material may also be tested. A density map is calculated after removing a soil component of measured abundances, wt % oxides being normalized to a Cl-free, H_2O, and S-free composition. The soil composition for this exercise is given in Table 2. The effect on the density calculation of removing up to 30 wt % of a soil component remains small (below 50 kg/m^3). Finally, we note that assuming all iron is in the ferrous state (Fe^{2+}) leads to a calculated density that is about 20 kg/m^3 higher than in the case of a Fe^{3+}/Fe_T ratio of 0.2.

In conclusion, and despite the large errors that are inherent in using GRS data to estimate pore-free densities, the obtained density values are in the range of 3200–3450 kg/m^3 and systematically above the previously proposed crustal density values of 2700–3100 kg/m^3. Lower density values would occur in the Noachian crust with a difference of ~100 kg/m^3 compared to Hesperian or Amazonian material. We note that this difference of density is consistent with the difference in elevation of the southern highlands under the assumption of Pratt isostatic compensation [*Belleguic et al.*, 2005].

4. Partial Melts of the Primitive Mantle

Further insights into the average density of the Martian crust are provided by considering the genetic link between the crust and the primitive Martian mantle. Regardless of the internal complexity of crustal structure and its degree of chemical heterogeneity, the bulk chemical composition of the secondary crust is the result of partial melting of a mantle source. A simple approach to estimate the bulk chemistry of secondary crustal material is to calculate the composition of melts extracted from a primitive mantle composition such as that proposed by *Dreibus and Wänke* [1985] (noted DW85). Application of this approach has been successful in reproducing chemical and mineralogical remote sensing observations [*Baratoux et al.*, 2011, 2013] such as variations in time of the bulk chemistry (Si, Fe, Th) and the relative abundance of high-calcium and low-calcium pyroxene related to mantle cooling over time.

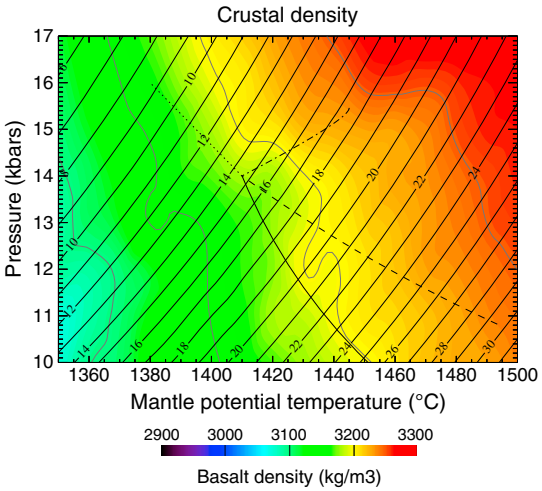

Figure 11. Density of crustal rocks estimated from equilibrium crystallization at the surface of primary melts of the Martian primitive mantle. Primary melts are calculated assuming equilibrium at the base of the lithosphere; conditions of partial melting are defined by pressure and mantle potential temperature [*Baratoux et al.*, 2013]. Oxygen fugacity is 3 log units below the QFM buffer for melting [*Herd et al.*, 2002] and 2 logs units below the QFM buffer for surface conditions. Labeled solid lines indicate the corresponding degree of partial melting. Dotted lines are possible thermal scenarios for the evolution of the Martian mantle from (right) the Noachian to (left) the Amazonian as given by *Baratoux et al.* [2011, 2013].

However, this simple scenario of partial melting of primitive mantle to form the Martian crust contrasts with the message from isotopic studies and the rare earth element chemistry of the basaltic shergottites that indicates the existence of distinct mantle chemical reservoirs [*Grott et al.*, 2013, *Mezger et al.*, 2013, and references herein]. Various processes, including the early formation of distinct geochemical reservoirs after magma ocean crystallization or formation of depleted residues following production of crustal material during the Noachian and Hesperian, could lead to the formation of a heterogeneous mantle. Evidence for a preserved primitive mantle reservoir is debated. Phase equilibrium experiments performed on a synthetic analog of the Adirondack-class basalts at Gusev by *Monders et al.* [2007] is consistent with the existence of a primitive mantle reservoir. This result that has been later questioned by *Filiberto et al.* [2008] as Humphrey (one of the Adirondack-class basalts) appears to be saturated with olivine and pigeonite (but not orthopyroxene). However, *Filiberto et al.* [2010] shows that Fastball, another basaltic rock at Gusev crater, is saturated with olivine and pyroxene and would be therefore in equilibrium with the primitive Martian mantle. While most of the lavas formed during the Hesperian could have been produced from a primitive source, the situation may be more complex for young lavas [*Baratoux et al.*, 2011], including, if they are indeed young, the basaltic shergottites. Thus, if the vast majority of the (secondary) crust was made at or before the Hesperian, calculation of partial melts of the DW85 composition is a valid approach.

The compositions of primary melts of the DW85 primitive mantle composition as a function of pressure and mantle potential temperature (T_p) were therefore estimated using the pMELTS thermodynamical calculator [*Ghiorso et al.*, 2002] corrected for application to the iron-rich Martian mantle [*El Maarry et al.*, 2009]. Grids calculated between 10 kbars and 17 kbars with 0.5 kbars steps and between T_p = 1350 °C and T_p = 1500°C with 1°C steps were already calculated in *Baratoux et al.* [2011] for an oxygen fugacity set to 3 log units below the QFM buffer, and the same grids were used in this study. These temperature and pressure conditions correspond to variable degrees of partial melting ranging from 2% to about 34% that cover the range of estimates using in situ compositions [e.g., *Monders et al.*, 2007; *Filiberto et al.*, 2010] or Martian meteorites [e.g., *Musselwhite et al.*, 2006]. The crystallization products of these liquids at surface conditions (1 bar, and oxygen fugacity 2 log units below the QFM buffer) were then determined using rhylolite-MELTS [*Ghiorso and Sack*, 1995; *Gualda et al.*, 2014] that has been tested for Martian composition [*Balta and McSween*, 2013]. The density of the mineral assemblage obtained at the solidus temperature was then calculated at 25°C for direct comparison with the other results presented in this paper (assuming a thermal expansivity of 2.5×10^{-5} K^{-1}).

The densities of mineral assemblages resulting from surface crystallization of primary mantle melts are represented in Figure 11 as a function of mantle potential temperature and pressures of formation. Primary melts extracted from large degrees of partial melting and/or equilibrated at shallow depths are relatively enriched in silica, resulting in a larger concentration of plagioclase and therefore a lower density relative to melts from small degrees of partial melting at large depth that would form dense olivine-rich assemblages at the surface. Episodes of crustal growth may correspond to evolving conditions of partial melting. The thermal scenario proposed by *Baratoux et al.* [2011, 2013] based on changes in chemistry and mineralogy of volcanic material with time is indicated as dotted lines in the potential temperature-pressure space

(Figure 11). For an increase of the lithosphere thickness with time, a change in volcanic rock density with age is expected with older crustal components having a lower density associated with a lower (olivine + pyroxene)/feldspar ratio.

In conclusion, the consideration of a genetic link between the basaltic crust and the primitive mantle of Mars suggests that most plausible densities would range from 3100 to 3200 kg/m^3. Density values below 3000 kg/m^3 would be obtained exclusively in the case of low-pressure formation of low-degree partial melts. Such conditions are far from the thermal scenario constrained by geochemical proposed by *Baratoux et al.* [2011]. In addition, they are certainly not the ones expected during the early stages of Mars, where intense volcanism would have been responsible for a large fraction of the basaltic component of the crust.

5. Discussion

5.1. Validity of the Extrapolation to the Entire Crust

Several important factors limit extrapolation of our density values estimated for the surface (remote sensing, in situ observations) or the near subsurface (Martian meteorites) to the entire crust of Mars. For example, a porosity of 10% reduces the bulk density from 3200 kg/m^3 to only 2880 kg/m^3. Comparison of the density of Apollo samples, lunar meteorites, and densities inferred from surface chemical observations with bulk crustal densities inferred from the GRAIL (Gravity Recovery and Interior Laboratory) mission indicates a porosity for the upper few kilometers of the lunar crust up to 20% with an average value of 12% [*Wieczorek et al.*, 2013]. For the case of the Moon, the low surface gravity, the absence of lithification processes, the continuous gardening and fracturing of the crust by impact events, and most importantly the absence of viscous deformation at low temperatures [*Wieczorek et al.*, 2013] offer various explanations for such high porosity values. We cannot definitively exclude that such a high porosity value also applies to the Martian crust; however, the higher-pressure gradient, the potentially larger crustal temperatures, and evidence for abundant effusive volcanic activity (except in the case of vesiculated basalts) argue for lower values of porosity. In addition, while the pores of lunar rocks does not contain any material, the porosity of the Martian crust may be filled by volatile species (including water/water ice), reducing the effect of crustal porosity on density. For instance, a 12% porosity reduces the density from 3200 kg/m^3 to 2816 kg/m^3, but to only 2926 kg/m^3 if the porosity is filled with H_2O.

Sedimentary or locally altered material in aqueous environments, including hydrous clays and sulfate-bearing rocks represent another possible low-density component of the Martian crust. While these deposits appear to be widespread in the Noachian crust [*Ehlmann et al.*, 2013; *Carter et al.*, 2013], they should not extend to large depths. The absence of clays in the ejecta of large impact craters confirms that deep materials (> 1 km) are generally clay poor [*Barnhart and Nimmo*, 2011]. Even in the presence of a 1 km thick sedimentary deposit, a simple calculation shows that the presence of sedimentary material cannot affect the average density of the crust by more than a few tens of kg/m^3.

The major issue regarding the extrapolation of surface rock density to the entire crust is finally the fact that the diversity of the available compositions of igneous material might not be necessarily representative of the average density of the bulk igneous crust [*McCubbin et al.*, 2008; *Filiberto et al.*, 2014]. If crustal growth resulted from progressive surface accumulation and intracrustal emplacement of extracted mantle melts, the crustal density profile may be comparable to that of the terrestrial oceanic crust. As the changes in density of the oceanic crust are mostly related to changes in porosity, degree of alteration, and metamorphic grade [*Carlson and Herrick*, 1990], we may also expect similar (but smaller) positive density gradients with depth. The presence at depth of pyroxene and olivine-rich cumulates (as suggested by the Martian meteorites sample collection) would also induce a positive density gradient with depth.

Alternatively, anorthositic material could represent a hidden low-density primary component of the ancient crust (highlands). A low-density crustal component is consistent with the suggestion of *Belleguic et al.* [2005] that the difference in elevation of the southern highlands is partially due to a Pratt compensation of its lower density relative to Hesperian or Amazonian volcanic material. Regional low-density values in the range of 2500–2900 kg/m^3 have also been obtained for regions in the highlands from localized gravity/topography admittance and correlation spectra [*McGovern et al.*, 2004]. Anorthositic terrains or felsic rocks are rare on Mars but have been identified from visible/near-infrared spectroscopy [*Carter and Poulet*, 2013; *Wray et al.*, 2013], and feldspar-rich rocks have been also identified by Mars Pathfinder [*Brückner et al.*, 2003] and recently at Gale Crater by the Curiosity rover [*Sautter et al.*, 2014].

Such outcrops could be either remnants of an ancient anorthositic crust (similar to the Moon) or the result of local igneous differentiation of plutonic bodies. The latter interpretation is largely favored as Mars should not have the required conditions for the formation of a plagioclase floatation crust [*Elkins-Tanton et al.*, 2005]. However, based on the preceding discussion, and the absence of abundant light material at the surface, low average density values for the Martian crust could be the result of a felsic or anorthositic crustal component that has been entirely or partially buried by volcanic material of basaltic composition in the late Noachian or Hesperian eras. In this respect, the correlation between the rare identified outcrops of felsic/anorthositic material and the largest concentration of feldspar inferred from GRS measurements and CIPW norm could reflect areas where this component is in the near subsurface, and/or excavated by impact craters. The density map from GRS data may then guide the search of additional feldspar and quartz-bearing rocks that would help us to understand the frequency and distribution of this material in the Martian crust. A crustal structure composed of dense basaltic lavas overlying felsic material would imply that ascending basaltic magmas have been able to overcome the density barrier generated by the low-density felsic crust, which is not an insuperable problem as indicated by the case of mare volcanism on the Moon. Indeed, pMELTS calculations indicate that the density of primary mantle melts at the liquidus ranges from 2700 kg/m^3 for melts equilibrated at shallow depth (1 GPa) up to 2850 kg/m^3 for melts equilibrated at 1.7 GPa that is close to the density of anorthositic material. Finally, the possible presence of a buried anorthositic crust would challenge current understanding of magma ocean crystallization scenarios in the inner solar system as the conditions for a floatation crust are thought to occur in the case of the Moon and Mercury, but not in the case of Mars [*Elkins-Tanton*, 2012].

5.2. Is a Dense Crust Compatible With the Moment of Inertia and Average Density of Mars?

Spherical models of the internal structure of Mars are essentially constrained by the average density of Mars and by the average moment of inertia factor [*Sohl et al.*, 2005]. The tidal potential Love number k_2 is not sensitive to the density of the Martian crust [*Sohl et al.*, 2005] and will not be considered here. These calculations have generally considered a low-density crust (2700–3100 kg/m^3). It is therefore necessary to determine if a dense crust is compatible with these constraints and to explore the implications for crustal thickness as well as for core radius and density.

For this purpose, the structure of Mars is approximated by a three-layer model, the crust, the mantle, and the core. The possible, though unlikely [*Khan and Connolly*, 2008], existence of a perovskite layer above the core is neglected as it should have only a small effect on the moment of inertia factor. As the average density of Mars is known with high accuracy (3935 $\pm$ 0.0004 kg/m^3 from *Esposito et al.* [1992]), the model is considered to have five free parameters, the mantle radius r_m, equal to the radius of Mars (R) minus the crustal thickness, the crustal density ρ_{cr}, the mantle density ρ_m, the core radius r_{co}, and the core density ρ_{co}. In *Sohl et al.* [2005], the mantle was treated as a layer with constant density. This contrasts with the seminal paper of *Sohl and Spohn* [1997] that suggested the existence of a thick basaltic crust (100–250 km) from a more sophisticated model of the internal structure including compression and thermal expansion. Indeed, the pressure gradient between the upper and lower mantle leads to substantial variations of density that significantly affects the moment of inertia. The consequence of neglecting the density gradient in the mantle will be discussed later. A linear dependence of mantle density with depth is introduced here:

$$\rho_m(r) = \alpha r + \beta \tag{1}$$

where the density gradient in the mantle is fixed. With these settings, the average density of Mars is given by:

$$\rho = \rho_{cr} + \rho_{co}\left(\frac{r_{co}}{R}\right)^3 + \left(\frac{r_m}{R}\right)^3(\beta - \rho_{cr}) + \frac{3\alpha}{4R^3}\left(r_m^4 - r_{co}^4\right) - \beta\left(\frac{r_{co}}{R}\right)^3, \tag{2}$$

and the moment of inertia factor of this spherical object is given by

$$\frac{I}{MR^2} = \frac{2}{5}\left[\frac{\rho_{cr}}{\rho} + \left(\frac{r_{co}}{R}\right)^5\left(\frac{\rho_{co} - \beta}{\rho}\right) + \left(\frac{r_m}{R}\right)^5\left(\frac{\beta - \rho_{cr}}{\rho}\right)\right] + \frac{\alpha}{3\rho R^5}\left(r_m^6 - r_{co}^6\right). \tag{3}$$

Equation (2) may be rewritten to express the core density as a function of the other free parameters (r_m, ρ_{cr}, β, and r_{co}):

$$\rho_{co} = \beta + \left(\frac{R}{r_{co}}\right)^3\left[\rho - \rho_{cr} - \left(\frac{r_m}{R}\right)^3(\beta - \rho_{cr}) - \frac{3\alpha}{4R^3}\left(r_m^4 - r_{co}^4\right)\right] \tag{4}$$

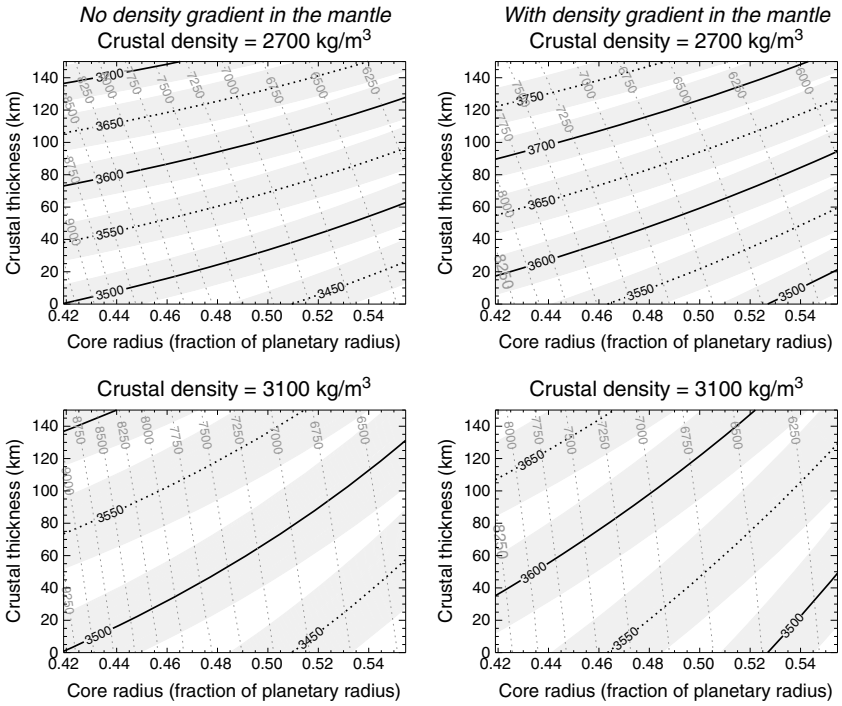

Figure 12. Acceptable solutions for core radius and crustal thickness based on a moment of inertia factor of 0.3635 ± 0.0012 and an average Mars density of 3935 kg/m^3. Corresponding average mantle densities are presented by solid or dotted black lines. The range of acceptable solutions for each mantle density (given the error bars on the moment of inertia factor) is delimited in grey. (left) The calculation neglects any density gradients within the mantle. (right) The calculation assumed a density gradient of 0.352 kg/m^3 per km in the mantle, based on *Khan and Connolly* [2008].

Equations (2) and (3) imply that the space of solution is three-dimensional (one parameter among r_m, ρ_{cr}, β, and r_{co} could be represented as a function of the three others).

In principle, additional constraints to this calculation may be conceived as the thickness of the crust, its density and the density of the residual mantle are petrogenetically related. Qualitatively, a thicker crust implies more extensive mantle melting, and therefore a lighter residual mantle (a few tens of kg/m^3). However, this effect is relatively small and the quantitative relation between the three variables is not unique as it depends on the details of crustal extraction (e.g., extent of melting with depth and degree of partial melting during the different episodes of crustal growth). Predictions could be made using pMELTS in the framework of a given scenario for crustal growth, but even in this case, errors on the relative stability of pyroxene and olivine at high pressure (above 1.5 GPa) precludes a precise estimation of the density of the residual mantle. It is therefore not recommended at this stage to include quantitative crust-mantle relationships based on petrological considerations in a more general inverse model. In practice, the 3-D subspace of solutions may be found by direct exploration of a four-dimensional space with reasonable bounds for r_{co}, r_m, ρ_{cr}, and β (or any other parameters representing the mantle density structure). In order to directly compare our results with *Sohl et al.* [2005], the average mantle density may be varied whereas β is related to the average mantle density through:

$$\beta = \overline{\rho_m} - \frac{3\alpha}{4}\left(\frac{r_m^4 - r_{co}^4}{r_m^3 - r_{co}^3}\right). \tag{5}$$

We recall here that *Sohl et al.* [2005] concluded from their calculation (with a constant density for the mantle) that the mantle is less dense with smaller iron content than previously thought.

A two-dimensional graph (crustal thickness versus core radius) for each crustal density may be used to represent the solutions (Figure 12). For a given average mantle density, acceptable values of crustal thickness and core radius appear as a domain delimited by the upper and lower bounds of the mean moment of inertia factor (0.3635 ± 0.0012 as in *Sohl et al.* [2005]). The corresponding core densities are then overplotted with labeled contours. Figure 12 shows the effect of omitting the density gradient in the mantle. Other

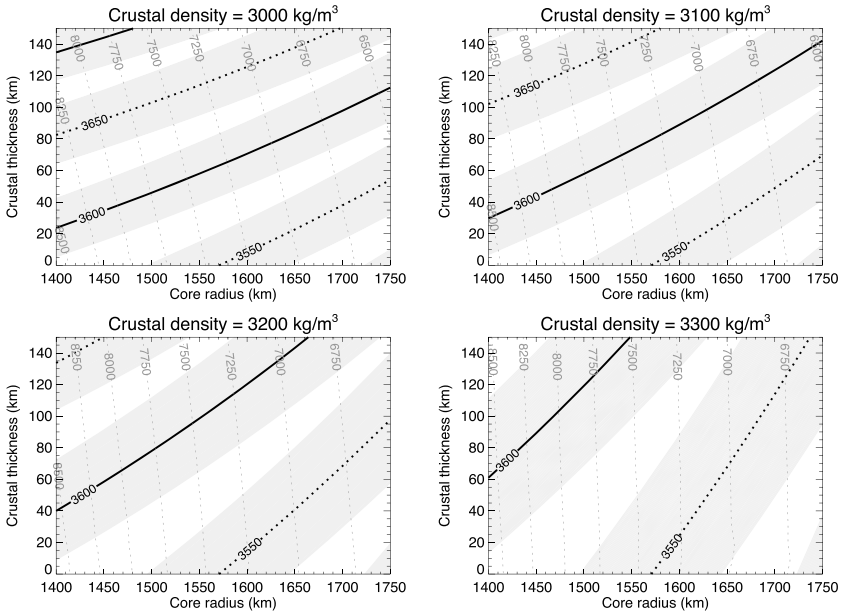

Figure 13. Considering a moment of inertia factor of 0.3635 ± 0.0012 and an average density of 3935 kg/m^3, the average mantle density as a free parameter and four different values of crustal densities from 3000 to 3300 kg/m^3, the acceptable solutions for the core radius and crustal thickness are represented. The corresponding average mantle densities are presented by solid or dotted black lines. The range of acceptable solutions for each mantle density given the error bar on the moment of inertia factor is delimited by a grey area. A density gradient of 0.352 kg/m^3 per km in the mantle, based on *Khan and Connolly* [2008], is used in all calculations.

assumptions are identical between this study and *Sohl et al.* [2005]. Core radius is represented as a fraction of the planetary radius allowing a direct comparison with *Sohl et al.* [2005]. A density gradient of 0.352 kg/m^3 per km has been used in the calculation [*Khan and Connolly*, 2008] and is in agreement with high-pressure experiments for a primitive Martian mantle composition [*Bertka and Fei*, 1997, 1998]. Neglecting this effect implies a change in mantle density of about 80 kg/m^3. This comparison invalidates the conclusion of *Sohl et al.* [2005] regarding the lower density and lower iron content of the mantle, if crust thickness and core size are specified. An iron-rich Martian mantle is therefore perfectly consistent with the mass and moment of inertia factor.

Figure 13 represents a broader exploration domain for crustal density and crustal thickness in comparison with previous studies (up to 3300 kg/m^3 and 200 km, respectively). These results imply that solutions with a high crustal density do exist and do not require any exotic values for core and mantle densities. In these calculations, the average mantle density is a free parameter. For the purpose of comparison with regional analysis of the gravity field that is sensitive to the density contrast at the crust-mantle interface, one can also perform similar calculations with the mantle density at the crust-mantle interface as a free parameter. In this case, the parameter β is related to the density of the mantle beneath the crust ($\rho_m(r_m)$) by

$$\beta = \rho_m(r_m) - \alpha r_m. \tag{6}$$

The results of the calculations are presented in Figure 14. The main implication is a reduced density contrast at the crust-mantle interface when considering a higher crustal density. Note that a higher density of the crust is easily compensated for by an increase of the core density and/or size to match the moment of inertia factor. While *Khan and Connolly* [2008] suggest a light core with high sulfur content (> 20 %), our higher density value for the core suggests a lower sulfur content that is more compatible with geochemical models of the Martian interior (Sulfur content of 14 wt %) [*Dreibus and Wänke*, 1985].

5.3. Is a Dense Crust Compatible With the Gravity Field of Mars?

Gravimetric methods have been used previously to constrain crustal thickness and density. Such inversions are generally nonunique with a noted tradeoff between these parameters. Using the measured ratio of the geoid and topography, it is possible to estimate the thickness of the crust, under the assumption that the

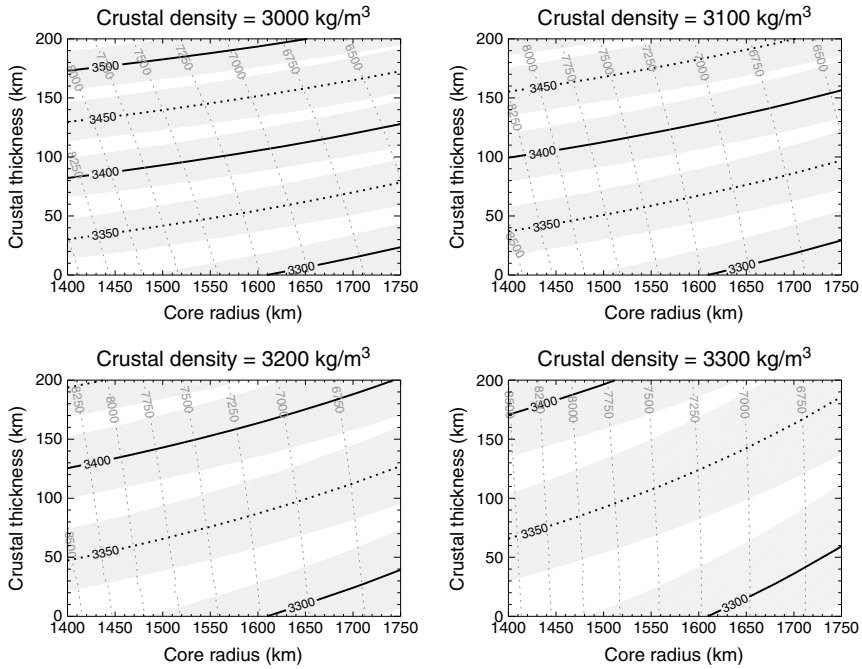

Figure 14. Considering a moment of inertia factor of 0.3635 ± 0.0012 and an average density of 3935 kg/m^3, the mantle density at the crust-mantle interface as a free parameter and four different values of crustal densities from 3000 to 3300 kg/m^3, the acceptable solutions for the core radius and crustal thickness are represented. The corresponding average mantle densities are presented by solid or dotted black lines. The range of acceptable solutions for each mantle density given the error bar on the moment of inertia factor is delimited in grey. A density gradient of 0.352 kg/m^3 per km in the mantle, based on *Khan and Connolly* [2008], is used in all calculations.

crust is uniform in density and is isostatically compensated. Assuming a range of crustal densities from 2700 to 3100 kg/m^3, the average thickness of the Martian crust in the highlands was estimated from this technique to be 57 ± 24 km [*Wieczorek and Zuber*, 2004]. For the highest density considered in that study, the average crustal thickness should be less than 67 km. Combining this global crustal thickness modeling, *Pauer and Breuer* [2008] obtained a maximum crustal density of 3020 ± 70 kg/m^3 for the highlands.

To address the consequences of crustal density on the thickness of the Martian crust, we have created a series of global crustal thickness maps using the most recent models of the Martian gravity field and topography. From these crustal models, we quantify the relationship between average crustal thickness and crustal density. Our modeling approach follows the procedure developed by *Wieczorek and Phillips* [1998] for the Moon that was later applied to Mars by *Wieczorek and Zuber* [2004] and *Neumann et al.* [2004]. For a given crustal density, the gravitational attraction of the surface topography (model MarsTopo719 [*Wieczorek*, 2007]) was calculated, taking into account finite-amplitude effects by using powers of topography to order 7. This field was subtracted from the observed gravity (JGMRO110C [*Konopliv et al.*, 2011]) to yield the Bouguer anomaly, which was subsequently truncated at spherical harmonic degree 90 given the dramatic decrease in spectral correlation that is observed between the observed gravity and topography beyond this degree. For a specified mantle density, and for a given average crustal thickness, the relief along the crust-mantle interface that best fits the Bouguer anomaly was determined in an iterative manner. To counteract the destabilizing effect where gravitational errors increase exponentially when continued downward, a filter was applied to the Bouguer potential that had a value of 0.5 at spherical harmonic degree 50 [e.g., *Wieczorek and Phillips*, 1998].

In our inversions, the minimum crustal thickness was always located in the central portion of the Isidis impact basin. After the iterative inversion converged, the average thickness of the crust was modified, and a new inversion performed, in order to obtain a solution where the minimum crustal thickness was equal to 1 km. This minimum thickness is a plausible estimate for the thickness of the postimpact lava flows and sediments that are found in this basin. Though it is not possible for the average thickness of the crust to be

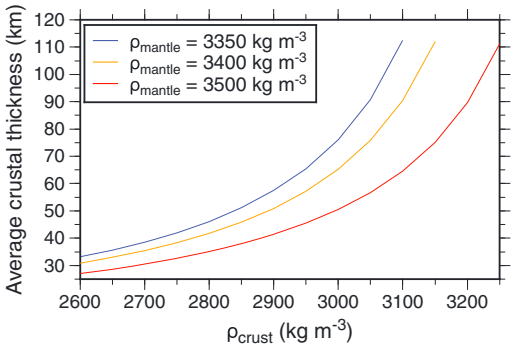

Figure 15. Average crustal thickness as a function of crustal density for three different mantle densities. For each crustal thickness inversion, the minimum crustal thickness was constrained to equal 1 km.

thinner than that obtained, if the thickness of the crust in the interior of the Isidis basin were greater than 1 km, the average crustal thickness would be thicker.

We plot in Figure 15 the average crustal thickness as a function of crustal density for three different plausible mantle densities: 3350, 3400, and 3500 kg/m^3 [*Bertka and Fei*, 1997, 1998]. Since the gravitational attraction of relief along the crust-mantle interface is proportional to the density contrast between the mantle and crust, as the mantle density decreases, the amplitude of the relief increases, and the average crustal thickness increases. As the density of the crust approaches the mantle density, the relief along the crust-mantle interface exceeds 200 km, at which point our crustal thickness inversions become unstable. The relations in this figure vary by less than 3 km when modifying the truncation degree and filter half-wavelength in our inversion. If the crustal density were as low as 2600 kg/m^3, perhaps as a result of impact induced fractures [e.g., *Wieczorek et al.*, 2013], the average crustal thickness could be as low as 27 km. For a crustal density of 2900 kg/m^3, the average crustal thickness is constrained to lie between 41 and 57 km, similar to previous work. For a crustal density of 3100 kg/m^3, the average crustal thickness is constrained to lie between 65 to about 110 km.

A dense and thick basaltic crust extracted from partial melting of a primitive mantle would be difficult to reconcile with mass balance models based on Nd-isotopic compositions of Martian meteorites [*Norman*, 1999] but would remain possible if depleted mantle source gave rise to additional secondary crustal materials [*Wieczorek and Zuber*, 2004]. On the other hand, average crustal thicknesses greater than about 70 km are inconsistent with the analysis of geoid-topography ratios [*Wieczorek and Zuber*, 2004; *Pauer and Breuer*, 2008] and crustal thickness in excess of ~100 km might lead to lower crustal flow and destruction of crustal thickness variations [*Nimmo and Stevenson*, 2001]. Nevertheless, we note that such analyses are based upon the crust having a constant density and that any form of vertical stratification in density could bias the obtained average crustal thickness [e.g., *Wieczorek and Phillips*, 1997].

5.4. Implication for the Recycling of the Martian Crust

In the absence of plate tectonics and subduction, recycling of the Martian crust into the mantle should occur mainly through crustal delamination. Crustal delamination could occur if the lower crust became denser than the mantle, and if the thermal and compositional parameters favored rheological decoupling of this gravitationally unstable layer [*Morency and Doin*, 2004; *Ueda et al.*, 2012; *Samuel et al.*, 2014]. In particular, the delamination of crustal roots is conceivable if a basalt-to-eclogite transition occurs within the Martian crust. The transition consists in the progressive consumption of plagioclase and appearance of garnet. The transition may start near 50 km to 70 km [*Babeyko and Zharkov*, 2000; *Papike et al.*, 2013]. Numerical models of the thermochemical evolution of Mars often predict crustal thicknesses significantly above this value (up to 200 km) offering favorable conditions for crustal delamination [e.g., *Breuer and Spohn*, 2006; *Keller and Tackley*, 2009]. However, crustal delamination appears less plausible for crustal thickness values of 50 $\pm$ 12 km inferred from topography and gravity models and a conservative crustal density of 2700–3100 kg m^3 [*Wieczorek and Zuber*, 2004] and has received limited support beyond the preliminary investigations of *Babeyko and Zharkov* [2000].

Arguments against the possibility of massive recycling of the Martian crust have been made based upon the geochemical analysis of Martian meteorites. Indeed, the Shergottites indicate an early separation of geochemical reservoirs that have not mixed since differentiation [*Papike et al.*, 2009; *Debaille et al.*, 2008; *Brandon et al.*, 2012]. These arguments have led *Morschhauser et al.* [2011] to select numerical models that do not allow crustal recycling, despite the fact that such models suggest that crustal recycling would be the rule rather than the exception. If the entire Martian crust has a composition that is similar to its surface, which is basaltic, then our reappraisal of possible density values suggests that the average crustal thickness would be comparable to or larger than the depth of the basalt-eclogite transition, reopening

the question of crustal recycling on early Mars and more generally throughout all its history. A possible control on crustal thickness by delamination has been proposed for the Earth, for instance in the case of the Archaean-Proterozoic Fennoscandian shield [*Kukkonen et al.*, 2008] and also for Venus [*Turcotte*, 1989; *James et al.*, 2013]. Furthermore, the delamination of a crustal root can be associated with an asthenospheric return flow responsible for magmatic activity, as proposed for several contexts of intraplate volcanism on Earth. Such a mechanism could offer an interesting alternative to plume-related volcanism for explaining the formation of recent basaltic flows on Mars (e.g., Central Elysium Planitia).

6. Conclusion

Since the last geophysical estimates of crustal thickness derived from topography and gravity models, abundant petrological observations on igneous rocks of the Martian crust, including chemical analyses of Martian meteorites, in situ analyses by the MER rovers, and remote sensing observations of surface chemistry (Mars Odyssey), are now available. Assuming the surface basaltic component is representative of the entire crust, these independent sources of information systematically point to a crustal density significantly above the range of density values assumed for the analysis of gravity and topography data. A dense crust is also consistent with the expected average density of rocks derived from a homogeneous primitive mantle of Mars. A dense crust is compatible with the constraints given by the mass of Mars and its moment of inertia factor, and with crustal thickness inversions from topography and gravity models as long as crust thickness approaches 100 km. Such a thick crust would allow the phase transition from basalt to eclogite to occur and offers the possibility for crustal recycling through delamination.

However, geoid-to-topography ratio are not compatible with large thicknesses for the southern hemisphere of Mars (the highlands) and rocks exposed at the surface are not necessarily representative of the entire crust. The comparison of petrological and geophysical constraints suggests the potential existence of a light crustal component buried under subsequent volcanic products in the southern hemisphere (highlands). This primary crustal component should be less dense than surface basalts. As the existence of highly porous materials is thought unlikely given the pressure-temperature conditions prevailing within the Martian crust, this light component may be composed of felsic or anorthositic material similar to the lunar anorthosites. The InSight mission will soon provide the first seismological constraints on the Martian interior and should offer a decisive test for the conclusions presented in this study.

Acknowledgments

This study has been supported by the French Programme National de Planétologie of INSU. H. Samuel acknowledges the funds from the from the Deutsche Forschungsgemeinschaft (project SA 2042/2-1). The bulk chemistry and mineralogy of Martian meteorites are freely available on the Mars Meteorite Compendium (http://curator.jsc.nasa.gov/antmet/mmc/). Topography and gravity models of Mars and Gamma-Ray-Spectrometer data are available on the Planetary Data System (http://pds-geosciences.wustl.edu/). Walter Kiefer and an anonymous reviewers helped us to improve the clarity of the manuscript. We acknowledge F. Nimmo for his careful editorial handling of the manuscript.

References

Arvidson, R. E., et al. (2006), Overview of the Spirit Mars Exploration Rover Mission to Gusev Crater: Landing site to Backstay Rock in the Columbia Hills, *J. Geophys. Res.*, *111*, E02S01, doi:10.1029/2005JE002499.

Babeyko, A. Y., and V. N. Zharkov (2000), Martian crust: A modeling approach, *Phys. Earth Planet. Inter.*, *117*, 421–435, doi:10.1016/S0031-9201(99)00111-9.

Balta, J. B., and H. Y. McSween Jr. (2013), Application of the MELTS algorithm to Martian compositions and implications for magma crystallization, *J. Geophys. Res. Planets*, *118*, 2502–2519, doi:10.1002/2013JE004461.

Baratoux, D., M. J. Toplis, M. Monnereau, and O. Gasnault (2011), Thermal history of Mars inferred from orbital geochemistry of volcanic provinces, *Nature*, *472*, 338–341, doi:10.1038/nature09903.

Baratoux, D., M. J. Toplis, M. Monnereau, and V. Sautter (2013), The petrological expression of early Mars volcanism, *J. Geophys. Res. Planets*, *118*, 59–64, doi:10.1029/2012JE004234.

Barnhart, C. J., and F. Nimmo (2011), Role of impact excavation in distributing clays over Noachian surfaces, *J. Geophys. Res.*, *116*, E01009, doi:10.1029/2010JE003629.

Belleguic, V., P. Lognonné, and M. Wieczorek (2005), Constraints on the Martian lithosphere from gravity and topography data, *J. Geophys. Res.*, *110*, E11005, doi:10.1029/2005JE002437.

Bertka, C. M., and Y. Fei (1997), Mineralogy of the Martian interior up to core-mantle boundary pressures, *J. Geophys. Res.*, *102*, 5251–5264, doi:10.1029/96JB03270.

Bertka, C. M., and Y. Fei (1998), Density profile of an SNC model Martian interior and the moment-of-inertia factor of Mars, *Earth Planet. Sci. Lett.*, *157*, 79–88, doi:10.1016/S0012-821X(98)00030-2.

Bouvier, A., J. Blichert-Toft, and F. Albarède (2009), Martian meteorite chronology and the evolution of the interior of Mars, *Earth Planet. Sci. Lett.*, *280*, 285–295, doi:10.1016/j.epsl.2009.01.042.

Bouvier, A., J. Blichert-Toft, and F. Albarède (2014), Comment on "Geochronology of the Martian meteorite Zagami revealed by U-Pb ion probe dating of accessory minerals" by Zhou et al., *Earth Planet. Sci. Lett.*, *385*, 216–217, doi:10.1016/j.epsl.2013.09.012.

Boynton, W. V., et al. (2007), Concentration of H, Si, Cl, K, Fe, and Th in the low- and mid-latitude regions of Mars, *J. Geophys. Res.*, *112*, E12S99, doi:10.1029/2007JE002887.

Brandon, A. D., I. S. Puchtel, R. J. Walker, J. M. D. Day, A. J. Irving, and L. A. Taylor (2012), Evolution of the Martian mantle inferred from the ^{187}Re–^{187}Os isotope and highly siderophile element abundance systematics of shergottite meteorites, *Geochim. Cosmochim. Acta*, *76*, 206–235, doi:10.1016/j.gca.2011.09.047.

Breuer, D., and T. Spohn (2006), Viscosity of the Martian mantle and its initial temperature: Constraints from crust formation history and the evolution of the magnetic field, *Planet. Space Sci.*, *54*, 153–169, doi:10.1016/j.pss.2005.08.008.

Britt, D. T., R. J. Macke, W. S. Kiefer, A. J. Irving, G. Hupé, and G. J. Consolmagno (2012), The density, porosity, and magnetic susceptibility of two recent meteorite falls: Tissint and Sutter's Mill, *Meteorit. Planet. Sci. Suppl.*, *75*, 5350.

Brückner, J., G. Dreibus, R. Rieder, and H. Wänke (2003), Refined data of Alpha Proton X-ray Spectrometer analyses of soils and rocks at the Mars Pathfinder site: Implications for surface chemistry, *J. Geophys. Res.*, *108*(E12), 8094, doi:10.1029/2003JE002060.

Carlson, R. L., and C. N. Herrick (1990), Densities and porosities in the oceanic crust and their variations with depth and age, *J. Geophys. Res.*, *95*, 9153–9170, doi:10.1029/JB095iB06p09153.

Carter, J., and F. Poulet (2013), Ancient plutonic processes on Mars inferred from the detection of possible anorthositic terrains, *Nat. Geosci.*, *6*, 1008–1012, doi:10.1038/ngeo1995.

Carter, J., F. Poulet, J.-P. Bibring, N. Mangold, and S. Murchie (2013), Hydrous minerals on Mars as seen by the CRISM and OMEGA imaging spectrometers: Updated global view, *J. Geophys. Res. Planets*, *118*, 831–858, doi:10.1029/2012JE004145.

Chennaoui-Aoudjehane, H. C., et al. (2012), Tissint Martian meteorite: A fresh look at the interior, surface, and atmosphere of Mars, *Science*, *338*, 785–788, doi:10.1126/science.1224514.

Consolmagno, I. M., and D. Britt (1998), The density and porosity of meteorites from the Vatican collection, *Meteorit. Planet. Sci.*, *33*, 1231–1241.

Coulson, I. M., M. Beech, and W. Nie (2007), Physical properties of Martian meteorites: Porosity and density measurements, *Meteorit. Planet. Sci.*, *42*, 2043–2054, doi:10.1111/j.1945-5100.2007.tb01006.x.

Debaille, V., Q.-Z. Yin, A. D. Brandon, and B. Jacobsen (2008), Martian mantle mineralogy investigated by the ^{176}Lu- ^{176}Hf and ^{147}Sm-^{143}Nd systematics of shergottites, *Earth Planet. Sci. Lett.*, *269*, 186–199, doi:10.1016/j.epsl.2008.02.008.

Dreibus, G., and H. Wänke (1985), Mars, a volatile-rich planet, *Meteoritics*, *20*, 367–381.

Ehlmann, B. L., G. Berger, N. Mangold, J. R. Michalski, D. C. Catling, S. W. Ruff, E. Chassefière, P. B. Niles, V. Chevrier, and F. Poulet (2013), Geochemical consequences of widespread clay mineral formation in Mars' ancient crust, *Space Sci. Rev.*, *174*, 329–364, doi:10.1007/s11214-012-9930-0.

El Maarry, M. R., O. Gasnault, M. J. Toplis, D. Baratoux, J. M. Dohm, H. E. Newsom, W. V. Boynton, and S. Karunatillake (2009), Gamma-ray constraints on the chemical composition of the Martian surface in the Tharsis region: A signature of partial melting of the mantle?, *J. Volcanol. Geotherm. Res.*, *185*, 116–122.

Elkins-Tanton, L. T. (2012), Magma oceans in the inner solar system, *Annu. Rev. Earth Planet. Sci.*, *40*, 113–139, doi:10.1146/annurev-earth-042711-105503.

Elkins-Tanton, L. T., P. C. Hess, and E. M. Parmentier (2005), Possible formation of ancient crust on Mars through magma ocean processes, *J. Geophys. Res.*, *110*, E12S01, doi:10.1029/2005JE002480.

Esposito, P. B., et al. (1992), Gravity and topography, in *Mars*, edited by H. H. Kieffer, 209 pp., Univ. of Arizona Press, Tucson, Ariz.

Filiberto, J., A. H. Treiman, and L. Le (2008), Crystallization experiments on a Gusev Adirondack basalt composition, *Meteorit. Planet. Sci.*, *43*(7), 1137–1146.

Filiberto, J., R. Dasgupta, W. S. Kiefer, and A. H. Treiman (2010), High pressure, near-liquidus phase equilibria of the Home Plate basalt Fastball and melting in the Martian mantle, *Geophys. Res. Lett.*, *37*, L13201, doi:10.1029/2010GL043999.

Filiberto, J., J. Gross, J. Trela, and E. C. Ferré (2014), Gabbroic Shergottite Northwest Africa 6963: An intrusive sample of Mars, *Am. Mineral.*, *99*, 601–606, doi:10.2138/am.2014.4638.

James, M. A., M. T. Zuber, and R. J. Phillips (2013), Crustal thickness and support of topography on Venus, *J. Geophys. Res. Planets*, *118*, 859–875, doi:10.1029/2012JE004237.

Ghiorso, M. S., and R. O. Sack (1995), Chemical mass transfer in magmatic processes IV. A revised and internally consistent thermodynamic model for the interpolation and extrapolation of liquid-solid equilibria in magmatic systems at elevated temperatures and pressures, *Contrib. Mineral. Petrol.*, *119*, 197–212, doi:10.1007/BF00307281.

Ghiorso, M. S., M. M. Hirschmann, P. Reiners, and V. I. Kress (2002), The pMELTS: A revision of MELTS for improved calculation of phase melting relations and major element partitionning related to partial melting of the mantle to 3 GPa, *Geochem. Geophys. Geosyst.*, *3*(5), 1030, doi:10.1029/2001GC000217.

Greeley, R., B. H. Foing, H. Y. McSween Jr., G. Neukum, P. Pinet, M. van Kan, S. Werner, D. A. Williams, and T. E. Zegers (2005), Fluid lava flows in Gusev crater, Mars, *J. Geophys. Res.*, *110*, E5008, doi:10.1029/2005JE002401.

Grott, M., et al. (2013), Long-term evolution of the Martian crust-mantle system, *Space Sci. Rev.*, *174*, 49–111, doi:10.1007/s11214-012-9948-3.

Gualda, G., M. Ghiorso, R. Lemons, and T. Carler (2014), Rhyolite-MELTS: A modified calibration of MELTS optimized for silica-rich, fluid-bearing magmatic systems, *J. Petrol.*, *53*, 875–890, doi:10.1093/petrology/egr080.

Herd, C. D. K., L. E. Borg, J. H. Jones, and J. J. Papike (2002), Oxygen fugacity and geochemical variations in the Martian basalts: Implications for Martian basalt petrogenesis and the oxidation state of the upper mantle of Mars, *Geochim. Cosmochim. Acta*, *66*, 2025–2036, doi:10.1016/S0016-7037(02)00828-1.

Hutchison, C. (1975), The norm, its variations, their calculations and relationships, *Schweiz. Mineral. Petrogr. Mitt.*, *55*, 243–256.

Keller, T., and P. J. Tackley (2009), Towards self-consistent modeling of the Martian dichotomy: The influence of one-ridge convection on crustal thickness distribution, *Icarus*, *202*, 429–443, doi:10.1016/j.icarus.2009.03.029.

Khan, A., and J. A. D. Connolly (2008), Constraining the composition and thermal state of Mars from inversion of geophysical data, *J. Geophys. Res.*, *113*, E07003, doi:10.1029/2007JE002996.

King, P., and S. McLennan (2010), Sulfur on Mars, *Elements*, *6*, 107–112, doi:10.2113/gselements.6.2.107.

Konopliv, A. S., S. W. Asmar, W. M. Folkner, Ö. Karatekin, D. C. Nunes, S. E. Smrekar, C. F. Yoder, and M. T. Zuber (2011), Mars high resolution gravity fields from MRO, Mars seasonal gravity, and other dynamical parameters, *Icarus*, *211*, 401–428, doi:10.1016/j.icarus.2010.10.004.

Kukkonen, I. T., M. Kuusisto, M. Lehtonen, and P. Peltonen (2008), Delamination of eclogitized lower crust: Control on the crust mantle boundary in the central Fennoscandian shield, *Tectonophysics*, *457*, 111–127, doi:10.1016/j.tecto.2008.04.029.

Lodders, K. (1998), A survey of SNC meteorite whole-rock compositions, *Meteorit. Planet. Sci. Suppl.*, *33*, 183–190.

McCubbin, F. M., H. Nekvasil, A. D. Harrington, S. M. Elardo, and D. H. Lindsley (2008), Compositional diversity and stratification of the Martian crust: Inferences from crystallization experiments on the picrobasalt Humphrey from Gusev Crater, Mars, *J. Geophys. Res.*, *113*, E11013, doi:10.1029/2008JE003165.

McGovern, P., S. Solomon, D. Smith, M. Zuber, M. Simons, M. Wieczorek, R. Phillips, G. Neumann, O. Aharonson, and W. Head (2002), Localized gravity/topography admittance and correlation spectra on Mars: Implications for regional and global evolution, *J. Geophys. Res.*, *107*(E12), 5136, doi:10.1029/2002JE001854.

McGovern, P., S. Solomon, D. Smith, M. Zuber, M. Simons, M. Wieczorek, R. Phillips, G. Neumann, O. Aharonson, and W. Head (2004), Correction to localized gravity/topography admittance and correlation spectra on Mars: Implications for regional and global evolution, *J. Geophys. Res.*, *109*, E07007, doi:10.1029/2004JE002286.

McSween, H. Y., et al. (2008), Mineralogy of volcanic rocks in Gusev Crater, Mars: Reconciling Mössbauer, Alpha Particle X-Ray Spectrometer, and Miniature Thermal Emission Spectrometer spectra, *J. Geophys. Res.*, *113*, E06S04, doi:10.1029/2007JE002970.

Meyer, C. (2012), Mars meteorite compendium [Available at http://curator.jsc.nasa.gov/antmet/mmc/.], *Tech. Rep.*, NASA.

Mezger, K., V. Debaille, and T. Kleine (2013), Core formation and mantle differentiation on Mars, *Space Sci. Rev.*, *174*, 27–48, doi:10.1007/s11214-012-9935-8.

Ming, D. W., et al. (2008), Geochemical properties of rocks and soils in Gusev Crater, Mars: Results of the Alpha Particle X-Ray Spectrometer from Cumberland Ridge to Home Plate, *J. Geophys. Res.*, *113*, E12S39, doi:10.1029/2008JE003195.

Monders, A. G., E. Médard, and T. L. Grove (2007), Phase equilibrium investigations of the Adirondack class basalts from the Gusev plains, Gusev crater, Mars, *Meteorit. Planet. Sci.*, *42*, 131–148, doi:10.1111/j.1945-5100.2007.tb00222.x.

Morency, C., and M.-P. Doin (2004), Numerical simulations of the mantle lithosphere delamination, *J. Geophys. Res.*, *109*, B03410, doi:10.1029/2003JB002414.

Morris, R. V., et al. (2006), Mössbauer mineralogy of rock, soil, and dust at Gusev crater, Mars: Spirit's journey through weakly altered olivine basalt on the plains and pervasively altered basalt in the Columbia Hills, *J. Geophys. Res.*, *111*, E02S13, doi:10.1029/2005JE002584.

Morris, R. V., et al. (2008), Iron mineralogy and aqueous alteration from Husband Hill through Home Plate at Gusev Crater, Mars: Results from the Mössbauer instrument on the Spirit Mars Exploration Rover, *J. Geophys. Res.*, *113*, E12S42, doi:10.1029/2008JE003201.

Morschhauser, A., M. Grott, and D. Breuer (2011), Crustal recycling, mantle dehydration, and the thermal evolution of Mars, *Icarus*, *212*, 541–558, doi:10.1016/j.icarus.2010.12.028.

Moser, D. E., K. R. Chamberlain, K. T. Tait, A. K. Schmitt, J. R. Darling, I. R. Barker, and B. C. Hyde (2013), Solving the Martian meteorite age conundrum using micro-baddeleyite and launch-generated zircon, *Nature*, *499*, 454–457, doi:10.1038/nature12341.

Musselwhite, D. S., H. A. Dalton, W. S. Kieffer, and A. H. Treiman (2006), Experimental petrology of the basaltic shergottite Yamato-980459: Implications for the thermal structure of the Martian mantle, *Meteorit. Planet. Sci.*, *41*(9), 1271–1290.

Neumann, G. A., M. T. Zuber, M. A. Wieczorek, P. J. McGovern, F. G. Lemoine, and D. E. Smith (2004), Crustal structure of Mars from gravity and topography, *J. Geophys. Res.*, *109*, E08002, doi:10.1029/2004JE002262.

Nimmo, F., and D. J. Stevenson (2001), Estimates of Martian crustal thickness from viscous relaxation of topography, *J. Geophys. Res.*, *106*(E3), 5085–5098, doi:10.1029/2000JE001331.

Nimmo, F., and K. Tanaka (2005), Early crustal evolution of Mars, *Annu. Rev. Earth Planet. Sci.*, *33*, 133–161, doi:10.1146/annurev.earth.33.092203.122637.

Norman, M. D. (1999), The composition and thickness of the crust of Mars estimated from rare Earth elements and neodymium isotopic compositions of Martian meteorites, *Meteorit. Planet. Sci.*, *34*, 439–449.

Papike, J. J., J. M. Karner, C. K. Shearer, and P. V. Burger (2009), Silicate mineralogy of Martian meteorites, *Geochim. Cosmochim. Acta*, *73*, 7443–7485, doi:10.1016/j.gca.2009.09.008.

Papike, J. J., P. V. Burger, C. K. Shearer, and F. M. McCubbin (2013), Experimental and crystal chemical study of the basalt-eclogite transition in Mars and implications for Martian magmatism, *Geochim. Cosmochim. Acta*, *104*, 358–376, doi:10.1016/j.gca.2012.11.007.

Pauer, M., and D. Breuer (2008), Constraints on the maximum crustal density from gravity topography modeling: Applications to the southern highlands of Mars, *Earth Planet. Sci. Lett.*, *276*, 253–261, doi:10.1016/j.epsl.2008.09.014.

Ringwood, A. E. (1966), Chemical evolution of the terrestrial planets, *Geochim. Cosmochim. Acta*, *30*, 41–104, doi:10.1016/0016-7037(66)90090-1.

Robie, R. A., and B. S. Hemingway (1995), Thermodynamic properties of minerals and related substances at 298.15 K and 1 bar (10^5 Pascals) pressure and at higher temperatures, *U. S. Geol. Surv. Bull.*, *2131*, 461–461.

Ruff, S. W., P. R. Christensen, D. L. Blaney, W. H. Farrand, J. R. Johnson, J. R. Michalski, J. E. Moersch, S. P. Wright, and S. W. Squyres (2006), The rocks of Gusev Crater as viewed by the Mini-TES instrument, *J. Geophys. Res.*, *111*, E12S18, doi:10.1029/2006JE002747.

Russell, C. T., et al. (2012), Dawn at Vesta: Testing the Protoplanetary Paradigm, *Science*, *336*, 684–686, doi:10.1126/science.1219381.

Samuel, H., D. Baratoux, and K. Kurita (2014), The early evolution of Mars' mantle and crust, in *International Interdisciplinary Workshop on: Accretion and Early Differentiation of the Terrestrial Planets*, Nice.

Sautter, V., et al. (2014), Igneous mineralogy at Bradbury Rise: The first ChemCam campaign at Gale crater, *J. Geophys. Res. Planets*, *119*, 30–46, doi:10.1002/2013JE004472.

Schmidt, M. E., et al. (2014), Geochemical diversity in first rocks examined by the Curiosity Rover in Gale Crater: Evidence for and significance of an alkali and volatile-rich igneous source, *J. Geophys. Res. Planets*, *119*, 64–81, doi:10.1002/2013JE004481.

Sohl, F., and T. Spohn (1997), The interior structure of Mars: Implications from SNC meteorites, *J. Geophys. Res.*, *102*(E1), 1613–1635, doi:10.1029/96JE03419.

Sohl, F., G. Schubert, and T. Spohn (2005), Geophysical constraints on the composition and structure of the Martian interior, *J. Geophys. Res.*, *110*, E12008, doi:10.1029/2005JE002520.

Solomon, S. C. (1980), Differentiation of crusts and cores of the terrestrial planets: Lessons for the early Earth?, *Precambrian Res.*, *10*, 177–194, doi:10.1016/0016-7037(66)90090-1.

Squyres, S. W., et al. (2003), Athena Mars rover science investigation, *J. Geophys. Res.*, *108*(E12), 8062, doi:10.1029/2003JE002121.

Squyres, S. W., et al. (2006), Overview of the Opportunity Mars exploration rover mission to Meridiani Planum: Eagle crater to Purgatory Ripple, *J. Geophys. Res.*, *111*, E12S12, doi:10.1029/2006JE002771.

Stolper, E. M., et al. (2013), The petrochemistry of Jake_M: A Martian mugearite, *Science*, *341*(6153), 1239463, doi:10.1126/science.1239463.

Taylor, G. J., et al. (2006), Variations in K/Th on Mars, *J. Geophys. Res.*, *111*, E03S06, doi:10.1029/2006JE002676.

Taylor, S. (2012), *Planetary Crusts: Their Composition, Origin and Evolution*, 402 pp., Cambridge Univ. Press, Cambridge.

Treiman, A. H., M. J. Drake, M.-J. Janssens, R. Wolf, and M. Ebihara (1986), Core formation in the Earth and Shergottite Parent Body (SPB): Chemical evidence from basalts, *Geochim. Cosmochim. Acta*, *50*(6), 1071–1091.

Treiman, A. H. (2003), Chemical compositions of Martian basalts (shergottites): Some inferences on basalt formation, mantle metasomatism, and differentiation in Mars, *Meteorit. Planet. Sci.*, *38*(12), 1849–1864.

Turcotte, D. (1989), Crustal deformation: Earth vs Venus, *Abstracts for the Venus Geoscience Tutorial and Venus Geologic Mapping Workshop*, p. 49, Lunar and Planetary Institute.

Ueda, K., T. V. Gerya, and J.-P. Burg (2012), Delamination in collisional orogens: Thermomechanical modeling, *J. Geophys. Res.*, *117*, B08202, doi:10.1029/2012JB009144.

Watters, T. R., P. J. McGovern, and R. P. Irwin III (2007), Hemispheres apart: The crustal dichotomy on Mars, *Annu. Rev. Earth Planet. Sci.*, *35*, 621–652, doi:10.1146/annurev.earth.35.031306.140220.

Weiss, B. P., and L. T. Elkins-Tanton (2013), Differentiated planetesimals and the parent bodies of chondrites, *Annu. Rev. Earth Planet. Sci.*, *41*, 529–560, doi:10.1146/annurev-earth-040610-133520.

Wieczorek, M. (2007), *Treatise on Geophysics*, chap. Gravity and topography of the terrestrial planets, vol. 10, pp. 165–206, Elsevier–Pergamon, Oxford.

Wieczorek, M. A., and R. J. Phillips (1997), The structure and compensation of the lunar highland crust, *J. Geophys. Res.*, *102*, 10,933-10,943, doi:10.1029/97JE00666.

Wieczorek, M. A., and R. J. Phillips (1998), Potential anomalies on a sphere—Applications to the thickness of the lunar crust, *J. Geophys. Res.*, *103*, 1715–1724, doi:10.1029/97JE03136.

Wieczorek, M. A., and M. T. Zuber (2004), Thickness of the Martian crust: Improved constraints from geoid-to-topography ratios, *J. Geophys. Res.*, *109*, E01009, doi:10.1029/2003JE002153.

Wieczorek, M. A., et al. (2013), The crust of the Moon as seen by GRAIL, *Science*, *339*, 671–675, doi:10.1126/science.1231530.

Wray, J. J., S. T. Hansen, J. Dufek, G. A. Swayze, S. L. Murchie, F. P. Seelos, J. R. Skok, R. P. Irwin, and M. S. Ghiorso (2013), Prolonged magmatic activity on Mars inferred from the detection of felsic rocks, *Nat. Geosci.*, *6*, 1013–1017, doi:10.1038/ngeo1994.

Zhou, Q., C. D. K. Herd, Q.-Z. Yin, X.-H. Li, F.-Y. Wu, Q.-L. Li, Y. Liu, G.-Q. Tang, and T. J. McCoy (2013), Geochronology of the Martian meteorite Zagami revealed by U-Pb ion probe dating of accessory minerals, *Earth Planet. Sci. Lett.*, *374*, 156–163, doi:10.1016/j.epsl.2013.05.035.

Zipfel, J., et al. (2011), Bounce Rock-A shergottite-like basalt encountered at Meridiani Planum, *Meteorit. Planet. Sci.*, *46*(1), 1–20, doi:10.1111/j.1945-5100.2010.01127.x.

Zuber, M. T. (2001), The crust and mantle of Mars, *Nature*, *412*, 220–227.